FILE

James Rennell Centre
for Ocean Circulation

INTERNAL DOCUMENT No. 16

Improving wind velocity measurements on ships

Industrial Training Year at the James Rennell Centre for Ocean Circulation 12 Aug 1993 - 9 Sept 1994

B I Moat

1994

UK
WOCE

Institute of
Oceanographic Sciences
Deacon Laboratory

Natural Environment Research Council

JAMES RENNELL CENTRE FOR OCEAN CIRCULATION

INTERNAL DOCUMENT No. 16

Improving wind velocity measurements on ships

Industrial Training Year at the James Rennell Centre for Ocean Circulation 12 Aug 1993 - 9 Sept 1994

B I Moat

1994

Gamma House
Chilworth Research Park
Chilworth
Southampton SO1 7NS
Tel 0703 766184
Telefax 0703 767507

ABSTRACT

Accurate wind speed measurements are required from Research vessels for satellite validation and climate research, but the results have been shown to differ significantly from ship to ship. This report discusses an attempt to find the cause of the discrepancies and, if possible, to correct for them.

A study on wind speed errors was undertaken to study the airflow distortions around a ship using numerical modelling. Simple potential models were used to study the airflow distortions around an idealised cylindrical mast to find the effect of the ship's mast on anemometers positioned close to it. The wake potential model was applied to wind speed data from R.R.S. Charles Darwin cruise 43 and partially corrected the wind speed measurements from anemometers at 5 to 6 mast diameters. The airflow distortions over the ship's hull and superstructure were then investigated to try to account for these remaining wind speed errors. Wind speed errors were calculated using a Computational Fluid Dynamics (C.F.D.) package and computer generated ship models. The study is in a preliminary stage and the C.F.D. package has been validated against a wind tunnel study for the C.S.S. Dawson and wind speed corrections agree to within 2 %.

IMPROVING WIND VELOCITY MEASUREMENTS ON SHIPS

1. INTRODUCTION

Accurate wind measurements at sea are required for satellite validation and climate research. The anemometers on Natural Environment Research Council, N.E.R.C., ships are very accurate, but the results differ from ship to ship. For example wind speed differences of up to 10 % appear in the results from the R.R.S. Charles Darwin when compared with the R.R.S. Discovery. The Meteorology team at the James Rennell Centre[1] also uses data from other sources, such as the French Research ship, the Suroit, and the Ocean Weather Ship Cumulus, both of which display possible systematic errors in wind speed. Section 2 discuses the quality of the data sets used in this study.

There are two possible causes of error in wind speed measurements; 1) the anemometer itself, and 2) disturbance of the flow of air at the anemometer site. The first of these was investigated by testing a typical anemometer in a wind tunnel (section 3). This approach could not be used to study the airflow since it would be too time consuming and extremely costly to build and wind tunnel test a model of every ship. Instead numerical modelling was used and the airflow distortions treated in two parts. In section 4, the airflow disturbance caused by the proximity of the ships mast to the anemometer is investigated using two potential flow models applied to an idealised mast (an infinitely long cylinder). The problem has been studied by many people such as (Kondo and Naito, 1972) and (Dabberdt, 1968). They compare their wind speed measurements to a simple potential model (section 4.2), and not to the realistic wake model of (Wucknitz, 1977), (section 4.3). The second cause of air flow disturbance is the effect of the ship itself, e.g. the air may lifted or accelerated over the bows of the ship, or may be blocked by the ships superstructure. This approach has been investigated using two dimensional numerical modelling by (Kahma and Lepparanta, 1981) on the Research Vessel Aranda and wind speed estimates where made to within 5% of those measured by an accurate bowsprit anemometer. This complex airflow problem is examined in greater detail using a three dimensional commercial Computational Fluid Dynamics package (section 5).

2. QUALITY CONTROL OF WIND SPEED DATA

2.1 Introduction

Wind speed data has been obtained from three six week R.R.S.. Discovery cruises, two cruises on R.R.S. Charles Darwin and one cruise on Le Suroit. All of these cruises used the fast

[1] A summary of the work of the James Rennell Centre is attached in Appendix A.

sampling Solent Sonic anemometer, plus other standard meteorological instrumentation, which are mounted on the foremast, which is situated in the bows of the ship. The data from R.R.S. Discovery is considered to be the best since the anemometer site has the best exposure, and because more cruises have been performed. The measurements made are therefore used as the standard in comparisons with other ships.

All research cruise data have already been processed. Figure 1 shows friction velocity, U* (the square root of wind stress), vs wind speed normalised to 10 m and reveal a possible 5% underestimate of wind speed by Le Suroit and an over estimate of 10% by R.R.S. Charles Darwin in comparison, to our R.R.S. Discovery standard. The friction velocity, U*, can be measured very accurately which leads us to believe that the errors occurring are due to errors in wind speed.

The O.W.S. Cumulus is situated at station LIMA (57 N 20 W), in the North Atlantic, which it holds four weeks in every five returning to Greenoch in Scotland to refuel and take on supplies. The Meteorological team has had instrumentation on board since 1987 which logs wind speed and direction via a Solent Sonic Anemometer and a Young Propeller Vane, pressure, position via a G.P.S. receiver and heading via a flux gate compass, and sea state information from a Ship Borne Wave Recorder. Cumulus experiences all weathers and logs data in two situations; 1) in moderate conditions it drifts with the port side exposed to the wind, and 2) in high wind speeds it 'hoves-to', were it steams slowly into the developing seas to ride out storms.

2.2 Method

The O.W.S. Cumulus data sets are received every month and are processed, checked and archived for future use. The processing is a standard procedure taken from the Cumulus data transfer/Processing instructions, refer to (Birch et al., 1993).

2.3 Quality of Data sets

Figure 2 shows friction velocity vs wind speed normalised to 10m for when Cumulus is drifting and hove to and it can clearly be seen that discrepancies of up to 30 % in wind speed occur. Although a lot of the Cumulus data is of lower quality than the research ships, it will be useful in future for testing the C.F.D. package, since the wind speed errors are larger than those experienced on other research ships. The Cumulus data set is also unique as measurements have been taken almost continuously at the same position for over seven years. In comparison to the data sets made on other research ships we have a large archived store of data with slightly larger wind speed errors, which will be reduced by the C.F.D. study, section 5, producing a large accurate data set.

Results form the wake potential model, section 4.3 and wind speed errors found from the C.F.D. study of the C.S.S. Dawson, section 5, have been used in a paper (Taylor et al. 1994) written for the COADS Winds Workshop presented in Kiel between

31st May till 2nd June 1994. The paper covers the accuracy of the O.W.S. Cumulus observations and the use of the O.W.S. Cumulus to validate wind estimates from the VOS Observing Programme - North Atlantic (VSOP-NA).

3. WIND TUNNEL STUDY OF AN ANEMOMETER

3.1 Introduction

All James Rennell Centre Cruises have a Solent Sonic Fast sampling Anemometer logging data. The Sonic anemometer is very accurate, around ± 1.5 % error for wind speeds < 30 m/s, but it is believed that the anemometer is designed to be mounted on stable platforms as the vertical axis calibration is not as thorough as the horizontal axis calibration. It was therefore decided to perform a wind tunnel study on a Solent Sonic anemometer that would soon be deployed on a Meteorological buoy in an experiment off the Welsh coast.

The anemometer was tested in the wind tunnel of Southampton University using a bracket that allowed the anemometer to be moved to all headings and elevations that could be encountered on a ship or buoy. The Solent sonic produced velocity readings in the x, y and z directions for each 10 degree angle and elevation over a 30 second period.

3.2 Method

This logged data was transferred onto the James Rennell Centre Sun network where it was converted into Pexec format which allows it to be easily manipulated using a library of over 200 Fortran routines. Areas of spurious data occurred as the anemometer was moved in the wind tunnel and these where removed by taking out data of a large standard deviation. The clean data was then averaged over each orientation for each elevation producing wind speed and directional errors.

3.3 Results

The results from the wind tunnel studies showed that the Solent Sonic anemometer was defective and was sent back to the suppliers to be re-calibrated.

4. AIR FLOW DISTORTIONS AROUND CYLINDRICAL MASTS

4.1 Introduction

It is well known that anemometers mounted close to towers or cylindrical mast can produce inaccuracies in wind speed measurements, therefore the position of an anemometer relative to this obstruction is critical in producing accurate wind speed measurements. R.R.S. Charles Darwin cruise 43 was undertaken to accurately measure wind stress using a number of fast sampling anemometers. The comparison of the wind speeds, (Yelland et al., 1991) , shows up discrepancies, some of which depend upon relative wind direction. This implies that the anemometers may feel the influence of the mast. The same problem has influenced the Royal Navy to undertake air flow trials on aircraft carriers. A large wind speed, or especially directional, error could mean that during night operations an aircraft could be launched from the wrong side of the ship causing the aircraft engine/transmission system to be over torqued. Increasing engine maintenance time, wasting fuel and increasing cost Wind speed errors were calculated from measurements made at an anemometer site and compared to a reference anemometer mounted on a 60 meter mast in an exposed position. These wind speed errors are available to us and could be used to validate the following two models.

The following section investigates the airflow distortion around an idealised cylindrical mast using two numerical models. The models are developed to show if wind speed errors can be explained by the air flow distortions found around the mast they are mounted on or are due to other effects such as the ships hull and superstructure. The two models developed are; 1) a simple potential flow model found in most fluid dynamics books (section 4.2), and 2) a realistic wake potential model built up from single complex equation, section 4.3 equation 11, given by (Wucknitz, 1977). The first model is too simple to model physical conditions and is used to form the basis of the second more relevant wake model. Section 4.4 applies wind speed corrections from the potential flow models to wind speed measurements made by R.R.S. Charles Darwin cruise 43.

4.2 Simple Potential Model

4.2.1 Introduction

This is a purely theoretical model of an ideal fluid which has zero viscosity. In this case the velocity potential ϕ and the stream function φ are defined as $\nabla^2\phi = 0$ and $\nabla^2\varphi = 0$ where ∇^2 is the Laplacian operator.

The flow field is symmetrical on either side of the cylindrical mast and it agrees closely with a flow of Reynolds number $Re < 10^{-1}$ and cylinder drag coefficient of about 50, which is entirely due to skin friction. This is known as a creeping flow and as the inertia forces are negligible the flow remains attached over the entire cylinder surface. Such flows occur in, for example, water seepage through a porous medium around a pipe.

It is hoped that some physical insight can be gained from this simple model with respect to the more complicated viscous flow.

4.2.2 The model

Velocity, direction and pressure are calculated in polar co-ordinates from a Cartesian grid of resolution (0.1,0.1) based on a mast diameter of one unit, which gave 10,251 grid points. The equations where built up using Pexec routines. Each addition and multiplication had to be applied to the grid points using a single Pexec routine. This was very slow, but gave an insight into the development of the more complex potential model.

The model is developed from a complex potential in three stages; 1) the velocity potential and stream function, 2) the velocity field, and 3) the pressure field.

As is well-known (e.g.. (Ditsworth and Allen, 1972)), the solution for the case of a static infinitely long cylinder of radius r_0 with undisturbed free stream velocity V_∞ is given by the complex potential

$$F(z) = V_\infty\left[z + \frac{r_0}{z}\right] \text{ where } z = x + iy \qquad (1)$$

$$\therefore F(z) = V_\infty\left[\text{Cos}\theta\left(r + \frac{r_0^2}{r}\right) + i\text{Sin}\theta\left(r - \frac{r_0^2}{r}\right)\right] \qquad (2)$$

which leads to a velocity potential of

$$\phi = V_\infty\left(\text{Cos}\theta\left(r + \frac{r_0^2}{r}\right)\right) \qquad (3)$$

and a stream function of

$$\varphi = V_\infty\left(\text{Sin}\theta\left(r - \frac{r_0^2}{r}\right)\right) \qquad (4)$$

see figure 3 which shows the equipotentials for velocity and stream lines.

where

V_∞ = free stream velocity. φ = stream function.

r = distance from cylinder centre. ϕ = velocity potential.

θ = angle to the flow. r_0 = mast radius.

refer to figure 5 which shows the model variables.

The velocities normal and tangential to the cylinder are calculated from the gradient of the velocity potential

$$V_n = \frac{\partial \phi}{\partial r} = V_\infty \mathrm{Cos}\theta\left(1 - \frac{r_0^2}{r^2}\right) \tag{5}$$

$$V_t = \frac{1}{r}\frac{\partial \phi}{\partial \theta} = -V_\infty \mathrm{Sin}\theta\left(1 + \frac{r_0^2}{r^2}\right) \tag{6}$$

and resolving the velocity into x and y components gives

$$V_x = V_\infty\left[\mathrm{Cos}^2\theta\left(1 - \frac{r_0^2}{r^2}\right) + \mathrm{Sin}^2\theta\left(1 + \frac{r_0^2}{r^2}\right)\right] \tag{7}$$

$$V_y = V_\infty\left[\mathrm{Sin}\theta\mathrm{Cos}\theta\left(1 - \frac{r_0^2}{r^2}\right) - \mathrm{Sin}\theta\mathrm{Cos}\theta\left(1 + \frac{r_0^2}{r^2}\right)\right] \tag{8}$$

$$Vel_C = V_\infty\sqrt{V_x^2 + V_y^2} \tag{9}$$

This model predicts that the flow is decreased both upwind and downwind of the cylinder. To either side the flow is increased, with a maximum occurring at 90 degrees to the free flow direction. On the cylinder surface at θ = 90 degrees the free stream velocity is doubled, decreasing to 4 % error at 5 mast radii and then decreasing to less than 1% at 10 mast radii. The percentage change from the free stream velocity is shown in figure 7 and the directional errors are shown in figure 9.

The ideal position for an anemometer in this model is at approximately θ = 45 and 135 degrees, where the calculated velocity is equal to the undisturbed free stream velocity.

The pressure field can be calculated from Bernoulli's equation.

$$\frac{P}{\rho} + \Phi_B + \frac{V^2}{2} - \frac{\partial \phi}{\partial t} = g(t)$$

Body forces (Φ_B) are neglected, $\frac{\partial \phi}{\partial t}$ = 0 for a constant velocity field and $g(t)$ becomes a constant.

ρ = density

P = pressure

V= Velocity

Leading to

$$P = P_\infty - \rho\frac{V_\infty^2}{2}\left[\frac{2r_0^2}{r^2}\left(\mathrm{Sin}^2\theta - \mathrm{Cos}^2\theta\right) + \frac{r_0^4}{r^4}\right] \tag{10}$$

where

P_∞ = Pressure at large distances from cylindrical mast

It can be shown that the flow has two stagnation points, where the velocity is zero, which are located on the surface of the cylinder upwind at θ = 180 degrees and downstream at θ = 0 degrees. These stagnation points correspond to maximum in the pressure field, whilst the minimum pressure is found on the cylinder surface at θ = 90 where the free stream velocity is doubled.

4.2.3 Summary

A velocity maximum is found at 90 degrees to the flow and a velocity decrease is shown upwind and downwind of the cylindrical body. The region of zero velocity error, or the ideal anemometer position, is located at 45 and 135 degrees to the flow. The model doesn't give a realistic interpretation of a physical atmospheric flow, because it uses a high drag coefficient (giving a very low Reynolds number) and is laminar everywhere within the flow.. Therefore the better airflow model will be the realistic turbulent wake region model described in section 4.3.

4.3 Wake Potential Model

4.3.1 Introduction

The following model was developed from a complex potential given by (Wucknitz, 1977).. It uses a point source near the centre of the mast and a point sink at a distance a downstream of the mast. This model differs from the simple potential model in that a wake is developed down stream of the mast, for a given cylindrical drag coefficient. This gives a more realistic interpretation of a flow for an atmospheric Reynolds number ($10^4 < Re < 10^7$). A theoretical treatment of the turbulent flow around a two dimensional cylindrical bodies has been given by (Hunt, 1973) and (Parkinson and Jandali, 1970).

4.3.2 The model

The velocity, direction and pressure fields are calculated and based on the same method as the simple potential model, except it is only possible to calculate the fields outside the mast and wake region. The model excludes all calculations within the wake because this region is known to exhibit turbulence and vortex shedding, which is chaotic in behaviour. The calculations are performed on the same grid and using the same resolution as the simple potential model. The equations where found too large to be manipulated using Pexec routines so both sets of model equations where written into a single Pexec routine giving repeated use and the same visualisation capabilities.

The only equations that exists for this model are the complex potential, equation 11, from (Wucknitz, 1977), the approximation to the mast and wake body, equation 14, and the relationship

$a = \frac{R}{2}$ which are both taken from (Wucknitz, 1980). The remaining equations have been developed during the duration of this project.

The complex potential for this model is

$$F(z) = V_\infty\left[z + \frac{Y_1}{\pi}\ln(z) - \frac{Y_2}{\pi}\ln(z-a)\right] \qquad (11)$$

$$= V_\infty\left[\phi + i\varphi\right]$$

where $z = x + iy$

which leads to a Velocity potential of

$$\phi = V_\infty\left[r_1\mathrm{Cos}\theta_1 + \frac{Y_1}{\pi}\ln(r_1) - \frac{Y_2}{\pi}\ln(r_3)\right] \qquad (12)$$

and a Stream Function of

$$\varphi = V_\infty\left[r_1\mathrm{Sin}\theta_1 + \frac{Y_1}{\pi}\theta_1 - \frac{Y_2}{\pi}\theta_3\right] \qquad (13)$$

see figure 4 which shows the equipotentials for velocity and stream lines.

where

$$r_1^2 = x^2 + y^2$$

$$\theta_1 = \mathrm{Tan}^{-1}\left(\frac{y}{x}\right)$$

$$r_3^2 = (x-a)^2 + y^2 = r_1^2 + a(a - 2r_1\mathrm{Cos}\theta_1)$$

$$\theta_3 = \mathrm{Tan}^{-1}\left(\frac{y}{x-a}\right) = \mathrm{Tan}^{-1}\left(\frac{r_1\mathrm{Sin}\theta_1}{r_1\mathrm{Cos}\theta_1 - a}\right)$$

Source intensity = $2V_\infty Y_1$ Sink intensity = $2V_\infty Y_2$ where $Y_1 > Y_2$

Refer to figure 6 which shows the model variables.

A better approximation to the mast and wake body is given by (Wucknitz, 1980) where

$$\varphi = Y_1 - Y_2 = R.C_D \qquad (14)$$

Y_1 and Y_2 are calculated from solving

$$\varphi = V_\infty\left[r_1\mathrm{Sin}\theta_1 + \frac{Y_1}{\pi}\theta_1 - \frac{Y_2}{\pi}\theta_3\right] = 0 \qquad (15)$$

substituting $Y_1 = R.C_D + Y_2$ from equation 14

gives

$$Y_2 = \frac{-\left(R.C_D.\theta_1 + \pi.r_1 Sin(\theta_1)\right)}{\left(\theta_1 - \theta_3\right)} \qquad (16)$$

Which gives a formula for calculating the value Y_2 along the contour $\varphi = R.C_D$.

The velocities normal and tangential to the cylinder are calculated from the gradient of the velocity potential

$$V_n = \frac{\partial\phi}{\partial r_1} = V_\infty\left[Cos\theta_1 + \frac{Y_1}{\pi r_1} - \frac{Y_2\left(r_1 - aCos\theta_1\right)}{\pi r_3^2}\right] \qquad (17)$$

$$V_t = \frac{1}{r_1}\frac{\partial\phi}{\partial\theta_1} = -V_\infty\left[Sin\theta_1\left(1 + \frac{Y_2 a}{\pi r_3^2}\right)\right] \qquad (18)$$

The source sink separation $a = \frac{R}{2}$ moves the centre of approximated cylinder downstream a distance a_0 (where $a_0 \propto C_D$) away from the origin of the co-ordinate system. To reduce this error in the velocity field the polar co-ordinate system must be calculated from this approximated mast centre using

$$V_n = \frac{\partial\phi}{\partial r_2} = V_\infty\left[Cos\theta_2 + \frac{Y_1}{\pi r_2} - \frac{Y_2\left(r_2 - aCos\theta_2\right)}{\pi r_3^2}\right] \qquad (19)$$

$$V_t = \frac{1}{r_2}\frac{\partial\phi}{\partial\theta_2} = -V_\infty\left[Sin\theta_2\left(1 + \frac{Y_2 a}{\pi r_3^2}\right)\right] \qquad (20)$$

where

$$r_2^2 = \left(x - a_0\right)^2 + y^2 = r_1^2 + a_0\left(a_0 - 2r_1 Cos\theta_1\right) \qquad (21)$$

$$\theta_2 = Tan^{-1}\left(\frac{y}{x - a_0}\right) = Tan^{-1}\left(\frac{r_1 Sin\theta_1}{r_1 Cos\theta_1 - a_0}\right) \qquad (22)$$

Refer to figure 6 which shows the model variables..

The velocity can be resolved into x and y components using

$$V_x = V_n Cos\theta_2 - V_t Sin\theta_2 \qquad (23)$$

$$V_y = V_n Sin\theta_2 + V_t Cos\theta_2 \qquad (24)$$

The region of maximum velocity is located downstream at 60 degrees to flow. The contour of the calculated wind velocity equal to the free stream velocity (i.e.. no velocity error) is located close to 100 degrees in the upstream region of the flow. This contour of the ideal anemometer location moves towards 90 degrees for decreasing drag cylindrical coefficient (C_D). Figures 8 and 10 show the percentage change from the free stream velocity and directional errors for a C_D of 1.0.

The contours of the wake region for varying cylindrical drag coefficient are shown in figure 11. The offset variable, a_0, can be approximated from this diagram and is shown, with corresponding Y_1 and Y_2 values, in table 1.

The pressure field can be calculated from

$$P = \left(\left(\frac{P_\infty}{\rho} + \frac{V_\infty^2}{2} \right) - \frac{\left(V_n^2 + V_t^2 \right)}{2} \right) \rho \qquad (25)$$

where

ρ = density

P_∞ = Pressure at large distances from the cylindrical mast.

Only one stagnation point occurs and is located upwind of the mast at θ = 180 degrees, where the velocity is zero and the pressure at a maximum.

4.3.3 Summary

The region of maximum velocity is moved downstream, from 90 degrees in the simple potential model to approximately 60 degrees in the wake potential model.

In comparison to the simple model the velocity decrease found upwind is approximately doubled when compared with the simple model and the contour of no velocity error moves from 135 degrees to close to 90 degrees to the flow. The wake potential model exhibits a realistic wake profile that is dependent on cylindrical drag coefficient and gives a more physical interpretation of airflow around a cylindrical mast.

4.4 Potential Models applied to R.R.S. Charles Darwin Cruise 43

4.4.1 Introduction

This study hopes to explain the wind speed discrepancies between measurements taken from research vessels and attribute these discrepancies to the anemometers proximity to a cylindrical mast. This section applies the wind speed corrections calculated from the potential models to wind speed measurements made on R.R.S. Charles Darwin cruise 43.

Charles Darwin cruise 43 was a joint Institute of Oceanographic Sciences Deacon Laboratory (I.O.S.D.L.) and the University of Manchester Institute of Science and Technology (U.M.I.S.T.) project to measure wind stress using a number of fast sampling wind sensors. The anemometers used were two fast sampling Sonic anemometers, the Solent Sonic and the Kaijo Denki Sonic, and three propeller anemometers, the RM Young Propeller vane, the RM Young Bi - Vane and the RM Young Tri - Axis anemometer. The only wind speed and direction data used are from those winds within $\pm$ 30 degrees of the Charles Darwin's bow. The anemometers are mounted close to a mast of 0.4 m

in diameter and situated in a well exposed position the bows of the ship. Refer to figure 12 and table 2 for their positions. No data is available for the Young Tri - Axis anemometer as one axis failed during the cruise.

4.4.2 Potential models applied to wind speed data from Charles Darwin Cruise 43

This study assumes that the anemometers do not to disturb the flow and are considered to be in the same plane (i.e.. vertical distortions are ignored). The model wind speed correction factors are produced for each anemometer from a Pexec program that calculates percentage wind speed error, percentage directional error and a scalar wind speed correction factor. These values are calculated for every one degree of relative wind direction and based on an input of cylindrical drag coefficient and distance to the anemometer. The wind speed data from Charles Darwin, normalised to 10 meters, is sorted on relative wind direction and the wind speed correction factors are applied. The comparisons of none model corrected wind speeds between different pairs of anemometers are plotted and a best line of fit is calculated for each pair. This is repeated for the model corrected wind speeds at different drags and the regression lines and regression coefficients are compared. The results are in three sections; 1) the model wind speed errors for each anemometer are shown, 2) the comparisons of none corrected wind speed to the model corrected wind speed for each anemometer are examined, and 3) the findings are discussed.

4.4.3 Results

The model wind speed and directional errors are shown in figures 13 to 22 and are discussed below.

The wind speed and directional errors are larger and more sensitive to change at those anemometer sites closest to the mast such as the Young Propeller Vane anemometer (figures 15 and 16) and the Young Bi Vane anemometer (figures 17 and 18). The Kaijo Denki Sonic anemometer (figures 21 and 22) is not so sensitive to change and shows a -4 % wind speed error, whilst the Solent Sonic anemometer (figures 13 and 14) and Tri - Axis anemometer (figures 19 and 20) show the lowest wind speed errors, between $\pm$ 2%. The largest errors are found at the Young Propeller Vane site, -10 % wind speed error and $\pm$ 4% directional error. The smallest errors are found at the Young Tri axis anemometer site, $\pm$ 2% wind speed error.

Table 3 shows the wind speed comparisons of the Solent Sonic and Young Propeller Vane. The gradient of the regression line for all the model corrected data, except for the simple potential model, has increased towards one and the offset has increased for all drag coefficients. This could imply that the model corrections give a good interpretation of the flow with an unexplained offset. The best gradient increase is in the comparisons of wind speed data at a drag of 1.2, see figure 21. The regression coefficient for the corrected wind speeds drops in comparison to the original data showing an increase in scatter which gives the impression the model isn't correcting the measurements.

The wind speed comparisons of the Solent Sonic and Kaijo-Denki Sonic are shown in table 4. The regression lines for all model corrected wind speeds are improved in comparison to the original

measured wind speed. The gradients are increased, the offsets are reduced and more significantly the regression coefficients are increased. The best line of fit is in the comparisons of wind speed data at a drag of 1.2, see figure 22. The potential model has improved the wind speed and has accounted for some of the errors.

The comparisons of the Kaijo-Denki and the Young Propeller Vane, refer to table 5, show worse regression lines for all model corrected data, an example is shown in figure 23. The model corrections have increased the wind speed errors and could imply that the Young Propeller Vane is being affected by objects not used in this study. For example, like railings and the open frame that runs the length of the mast.

The Solent Sonic and the Young Propeller Vane are mounted at different distances, the Solent Sonic at 2.4083 m and the Young Propeller Vane at 1.1180 m. The Young Propeller Vane is the closest anemometer to the mast and is considerably more sensitive to the mast and objects mounted on the mast. Which could explain the models inability to explain the errors in comparisons made using the Young Propeller Vane. The distances from the mast of the Solent Sonic anemometer and the Kaijo-Denki are large and quite similar, Solent Sonic at 2.4083 m and the Kaijo Denki at 2.3345 m, giving both good exposure. The model accounts some wind speed errors in these comparisons and attributes them to the airflow distortion around the mast. There are still unexplained wind speed errors in the data which could be explained by the airflow modelling in section 5.

4.5 Conclusions

From the potential flow study of Charles Darwin cruise 43 it becomes clear that the airflow distortion around the mast doesn't explain all the errors in the comparisons. The potential models don't take into account the effect of the anemometers on the flow and they also don't take into account the vertical distortion in the flow. The wake potential model is realistic in it's behaviour, but it only considers the air flow in a horizontal plane around an idealised mast. This could prove significant, possibly accounting for some more of the errors in the comparisons, and is measured in studies by (Mollo-Christensen, 1979) and (Kondo and Naito, 1972), but I believe that the major unexplained errors are due to the airflow over ships hull and superstructure and section 5 will give us the corrections needed to produce even higher quality wind speed data sets.

5. AIR FLOW DISTORTIONS OVER THREE DIMENSIONAL SHIP MODELS

5.1 Introduction

This study proposes to produce a quantitative error for the wind speed measurements from a simulated boundary layer flow within a Computational Fluid Dynamics package.

We are considering eight vessels. The N.E.R.C. research vessels, R.R.S. Charles Darwin. R.R.S. Discovery and R.R.S. Challenger, which measurements have been taken from. The French

vessel Le Suriot, which has also been used, and the Canadian research vessels C.S.S. Dawson and C.S.S. Hudson which we have wind tunnel results for. The O.W.S. Cumulus and lastly the M.O.D. buoy deploying vessel The Warden. All the Ship models are shown in appendix B.

A number of Computational fluid Dynamics (C.F.D.) packages have been researched and Ricardo Engineering agreed to do a preliminary study of the C.S.S. Dawson. This gave us the opportunity to evaluate the Ricardo C.F.D. wind tunnel results of the C.S.S. Dawson using the wind tunnel study carried out by (Thiebaux, 1990).

5.2 The ship models

From initial consultation with Ricrado Engineering it was decided to create our ship models using a pre-processor called Femgen. The Ricardo Finite element code, Vetis, has an interface with this pre-processor and also possesses an automatic mesh generating technique which is directly applicable to Femgen models. The Femgen package was installed at the James Rennell Centre and each model took approximately three weeks to make, starting from the two dimensional ship plans. The Vectis code uses a numerical three dimensional fluid dynamics model to calculate velocity vectors, pressure, temperature, turbulent velocity. It displays these results in colour shaded planes.

Two dimensional information for each ship was obtained and was digitised into auto-cad and saved in IGES format. The digitised two dimensional plans were read into Femgen and then each point could be easily be manipulated to the correct height, either by moving a whole section of points vertically or as was the case, each in turn. The information from the plans only contained horizontal sections at the deck level, main deck level and at the lower deck level, no information was available for the waterline section. This had to be interpolated from the two adjacent sections. The hulls of the vessels are symmetrical, whilst the superstructures are generally asymmetrical. This means that the hulls can be simply mirror imaged in Femgen to produce the whole hull, therefore only half the ships hull was digitised in Auto-Cad to save time.

In this way a line structure of the ship was built up until the meshing staged was reached. The Vectis code needs a three noded triangular mesh to be applied to the surface of the ship. This is achieved by defining surfaces using three or four points and then mesh generating these surfaces using the relevant mesh type. The mirroring process tended to double up points down the mirroring plane causing some surfaces to overlap. This was spotted by Ricardo when the finished model of the C.S.S. Dawson was sent to them for evaluation.

The accuracy of the ships generated within Femgen are dependent on the ship plans they have been generated from and at the time of writing this report the only results available are those carried out by Ricardo on the C.S.S. Dawson, refer to (Ricardo, 1994).

5.3 C.S.S. Dawson

The C.S.S. Dawson has two anemometer sites, one situated on a mast in the bows in a well exposed position and the other above the superstructure. Figure 26 shows the surface geometry and locations of the anemometer sites.

The bow anemometer is situated 1m back from the bow and 12.5 meters above the water line whilst the main anemometer is located 38.58 m from the bow, offset to port by 1.8 m and is 18.8 m above the water line. The study by (Thiebaux, 1990) also includes two test anemometer positions at heights of 2 m and 1 m above and below the bow anemometer site. At the time of writing this report the Vetis code didn't incorporate multiple monitoring locations so no results are available from these test anemometer locations.

5.4 Results

The results obtained by Ricardo with the C.S.S. Dawson head to wind show errors of 1% for the bow anemometer and 7.6% for the main anemometer. These results are very accurate in comparison to a bow anemometer wind speed error of -1% and a main anemometer wind speed error of 7% found by (Thiebaux, 1990). The wind speeds and directions over the C.S.S. Dawson are shown in Figure 27 taken from (Ricardo, 1994). This is at only one heading as the C.P.U. time needed to obtain this result is about a week. An over all processing time of around 12 weeks is needed to obtain a set of wind speed corrections every five degrees at $\pm$ 30 of a ships bow.

6. SUMMARY

The wake potential model used by J. Wucknitz and developed in this study can describe realistic velocity fields around a cylindrical mast. The model has been used to partially corrected wind speed errors for anemometers mounted close to a mast of 0.4m in diameter mounted on Charles Darwin cruise 43. The remaining wind speed errors have been attributed to the potential models inability take into account the air flow distortions caused by the anemometers themselves, the vertical airflow distortions around the mast and the effect of the ships hull and superstructure. This has been undertaken by using a commercial Computational Fluid Dynamics package to calculate wind speed errors from three dimensional computer generated ship models, and results from the C.S.S. Dawson model show an agreement to within 2% of wind tunnel studies.

The C.F.D. code is being installed at the James Rennell Centre and will be used to finish of the correction errors for the C.S.S. Dawson and calculate the wind speed correction errors for the Natural Environment Research Councils research vessels R.R.S. Discovery, R.R.S. Charles Darwin, R.R.S. Challenger, O.W.S. Cumulus, C.S.S. Hudson, Le Suriot and M.O.D. The Warden.

Future work is to compare the potential models to Navy data for further validation. Interest has been also shown in the James Rennell Centre creating ship models of the VOS Observing Programme - North Atlantic (VSOP-NA) fleet and using a Computational Fluid Dynamics package to study airflow distortions at the anemometer sites.

7. ACKNOWLEDGEMENTS

Dr. P.K. Taylor, Margaret Yelland, Vic Cornell.

8. REFERENCES

Birch, K. G., M. J. Yelland and S. K. Ward, 1993: Cumulus data transfer/processing instructions (Unpublished Report). , James Rennell Centre, Southampton, U.K., pp. .

Dabberdt, W. F., 1968: Wind disturbance by a vertical cylinder in the atmospheric surface layer. J. Appl. Meteorol., 7, 367-371.

Ditsworth, R. L. and T. Allen, 1972: Fluid mechanics, .McGraw-Hill, Kogakusha, pp. 415.

Gill, G. C., L. E. Olsson, J. Sela and M. Suda, 1967: Accuracy of wind measurements on Towers or Stacks. Bulletin American Meteorological Society, 48, 665-674.

Hunt, J. C. R., 1973: A theory of turbulent flow round two-dimensional bluff bodies. J. Fluid Mech., 61, 625-706.

Kahma, K. K. and M. Lepparanta, 1981: On errors in wind speed observations on R/V Aranda. Geophysica, 17(1-2), 155-165.

Kondo, J. and G. Naito, 1972: Disturbed Wind Fields around the Obstacle in Sheared Flow near the Ground Surface. J. Meteorol. Soc Japan, 50(2), 346-354.

Mollo-Christensen, E., 1979: Upwind distortion due to probe support in Boundary-Layer observation. J. Appl. Meteorol., 18, 367-370.

Parkinson, G. V. and T. Jandali, 1970: A wake source model for bluff body potential flow. J. Fluid Mech., 40, 577-594.

Ricardo, 1994: CFD analysis of airflow over the C.S.S. Dawson. (Unpublished Report). , Ricardo Consulting Engineers. Shoreham, U.K., pp. .

Taylor, P. K., E. C. Kent, M. J. Yelland and B. I. Moat, 1994: The accuracy of wind observations from ships. To be published in Proceedings of COADS Winds Workshop, May 1994, Kiel.

Thiebaux, M. L., 1990: Wind tunnel experiments to determine correction functions for shipboard Anemometers. , Canadian Contractor Report of Hydrography an Ocean sciences, Bedford Institute of Oceanography, Dartmouth, Novia Scotia, pp. .

Wucknitz, J., 1977: Disturbance of wind profile measurements by a slim mast. Boundary layer Meteorology, 11, 155-169.

Wucknitz, J., 1980: Flow distortion by Supporting Structures. : Air sea Interaction. Instruments and Methods, F. Dobson, L. Hasse and R. Davis, Ed., Plenum Press, 605 - 626.

Yelland, M. J., P. K. Taylor, K. G. Birch, R. W. Pascal and A. L. Williams, 1991: Evaluation of a Solent Sonic anemometer on R.R.S. Charles Darwin Cruise 43., Institute of Oceanographic Sciences Deacon Laboratory, 55 pp.

9. FIGURES

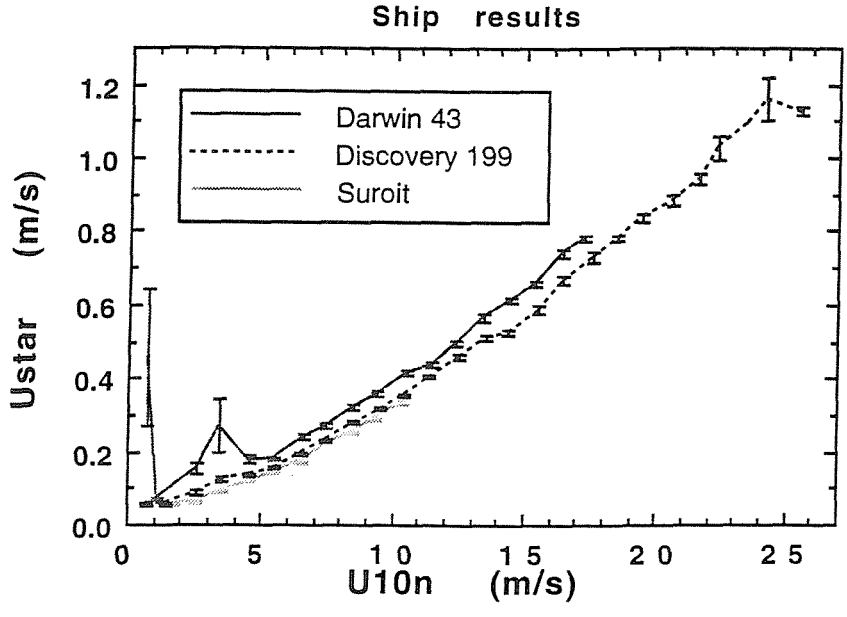

Figure 1 Comparison of friction velocity (U*) against normalised wind speed (U10n) showing wind speed discrepancies between R.R.S Charles Darwin, R.R.S. Discovery and Le Suroit.

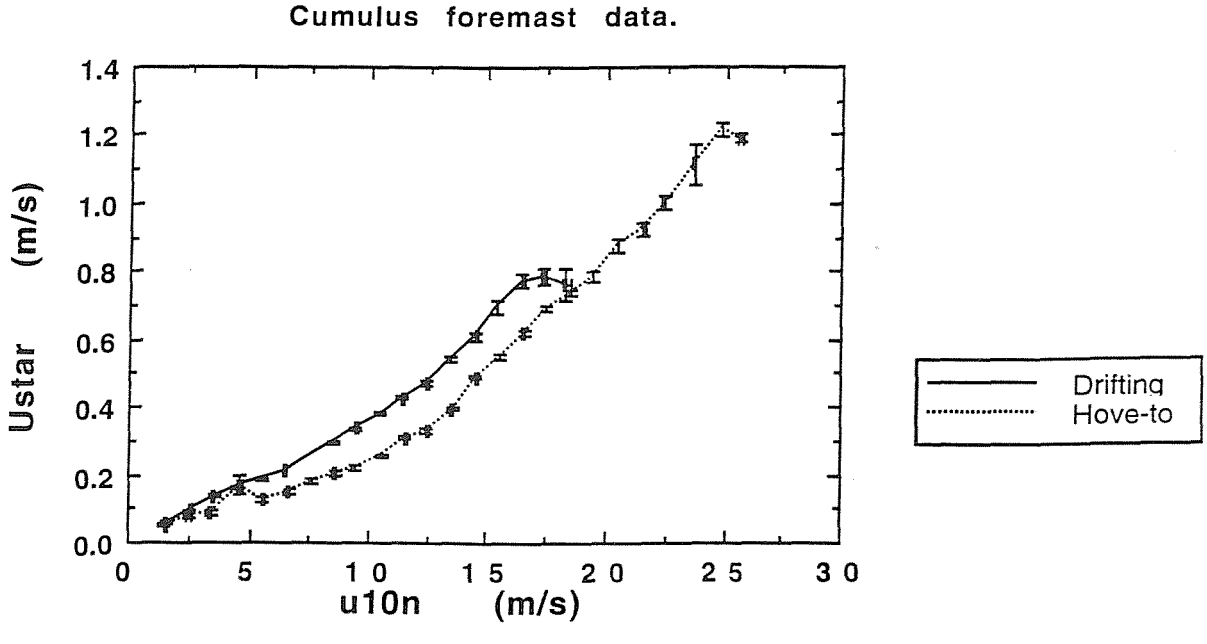

Figure 2 Comparison of friction velocity (Ustar) against normalised wind speed to 10 meters (U10n) showing wind speed discrepancies when the O.W.S. Cumulus is drifting and hove-to.

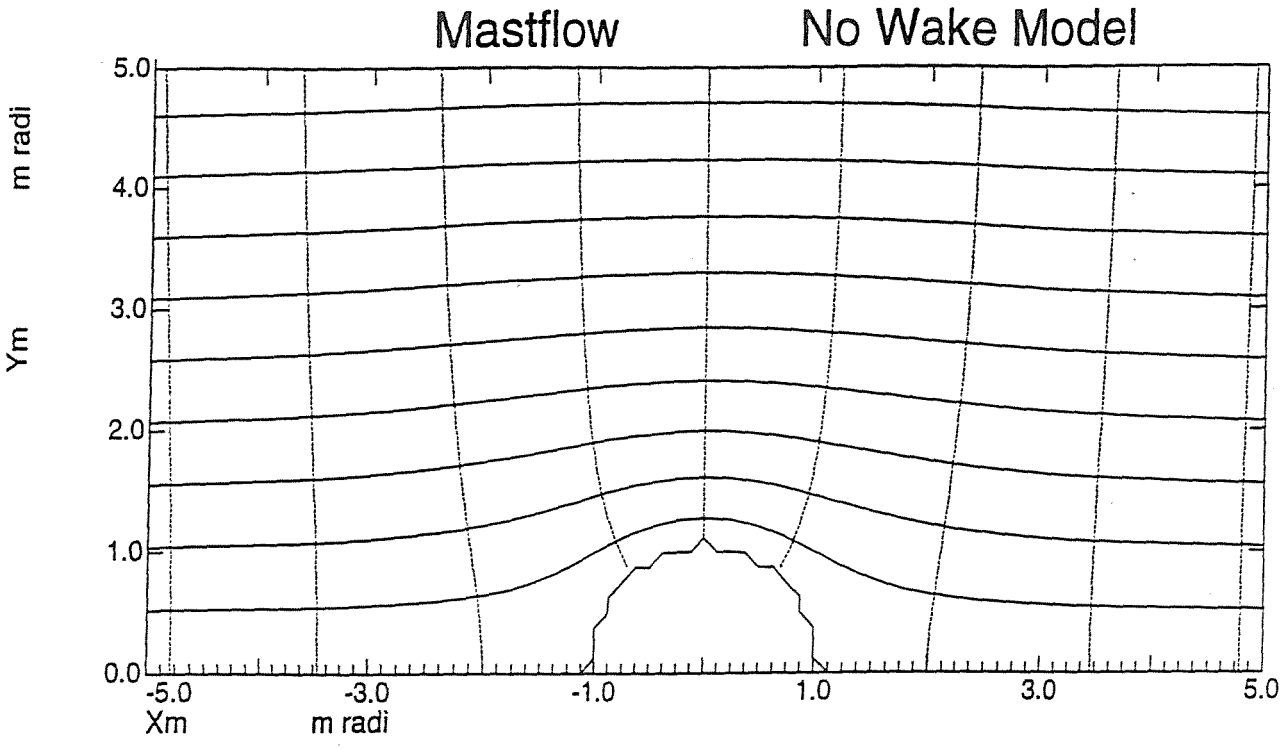

Figure 3 The solid and dashed lines respectively show the stream lines and equipotentials (for the no wake solution) around a mast of unit radius with the free stream entering from the left.

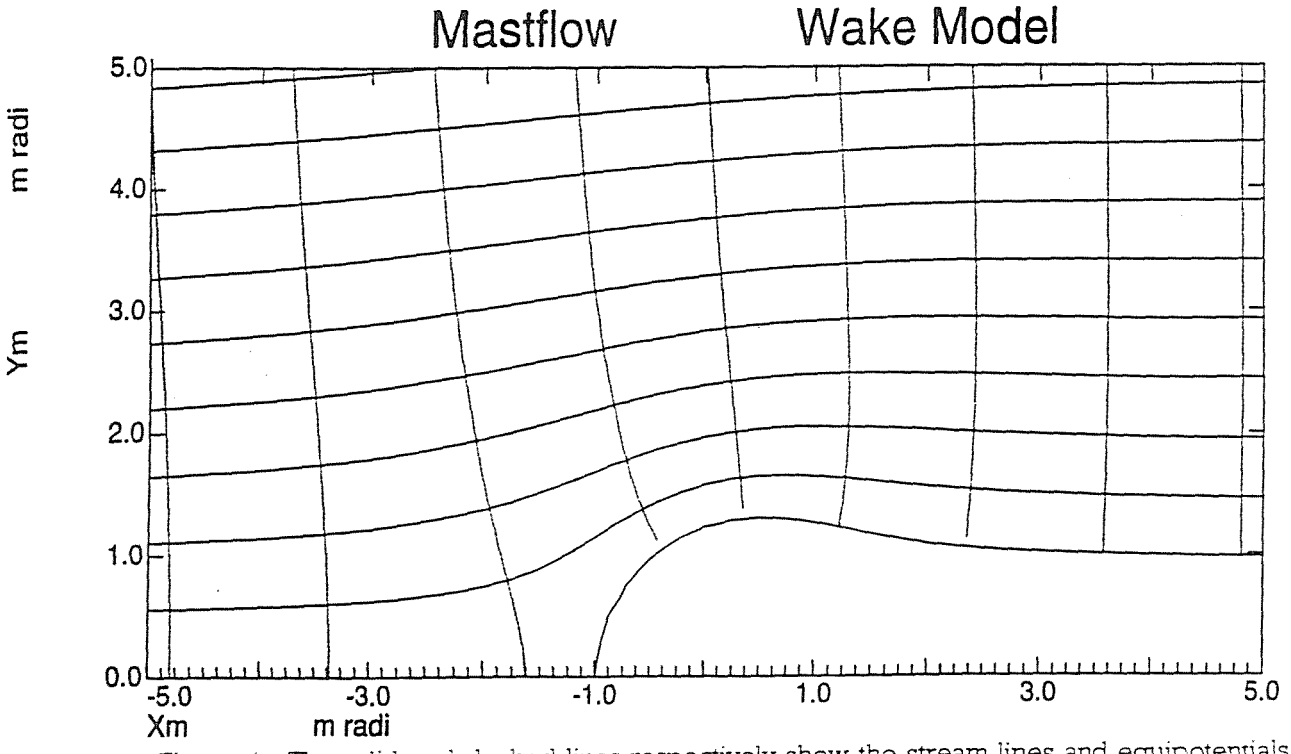

Figure 4 The solid and dashed lines respectively show the stream lines and equipotentials (for the wake solution where $C_D=1.0$) around a mast of unit radius with the free stream entering from the left..

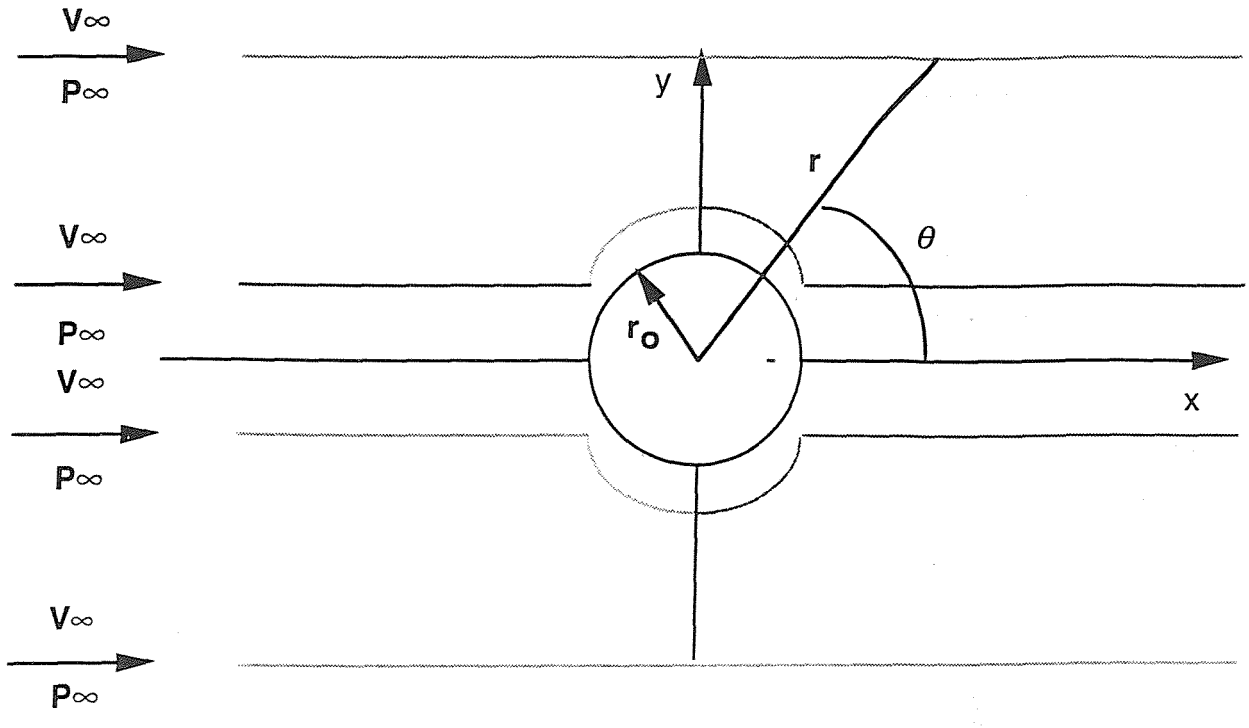

Figure 5 The variables in calculating the simple potential solution of an airflow around a cylindrical mast.

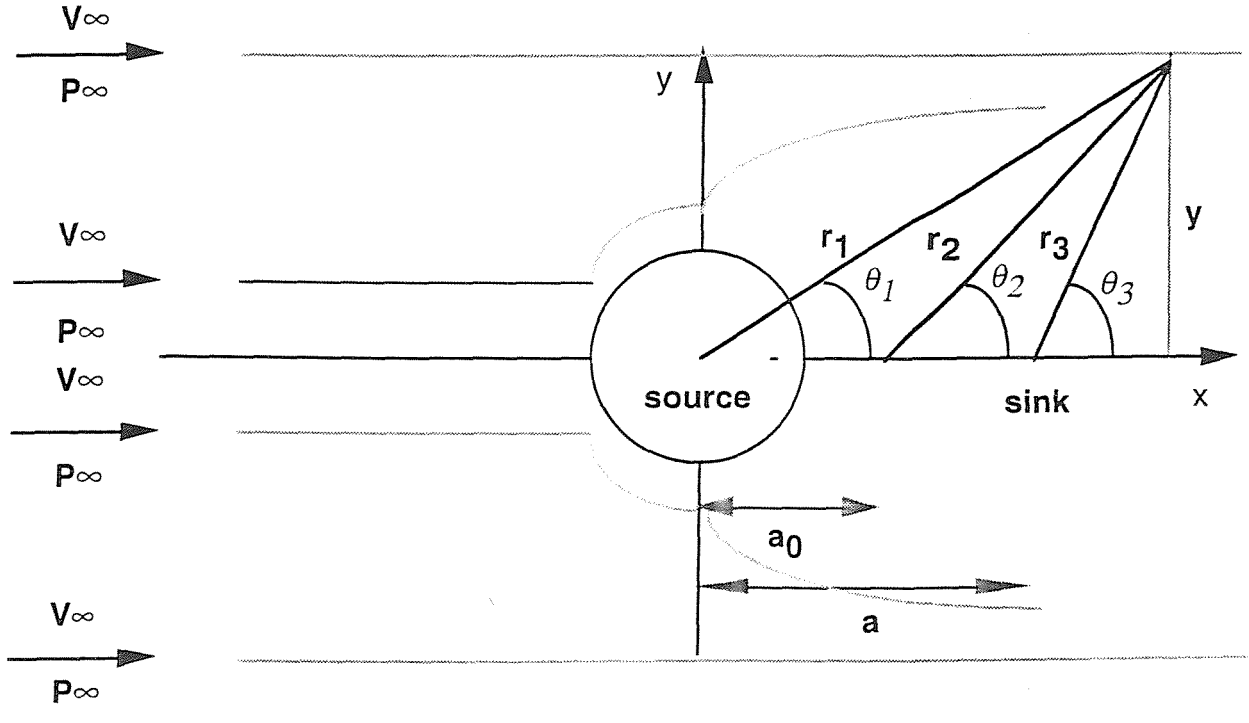

Figure 6 The variables used in calculating the potential solution of an airflow around a cylindrical mast with wake region downstream.

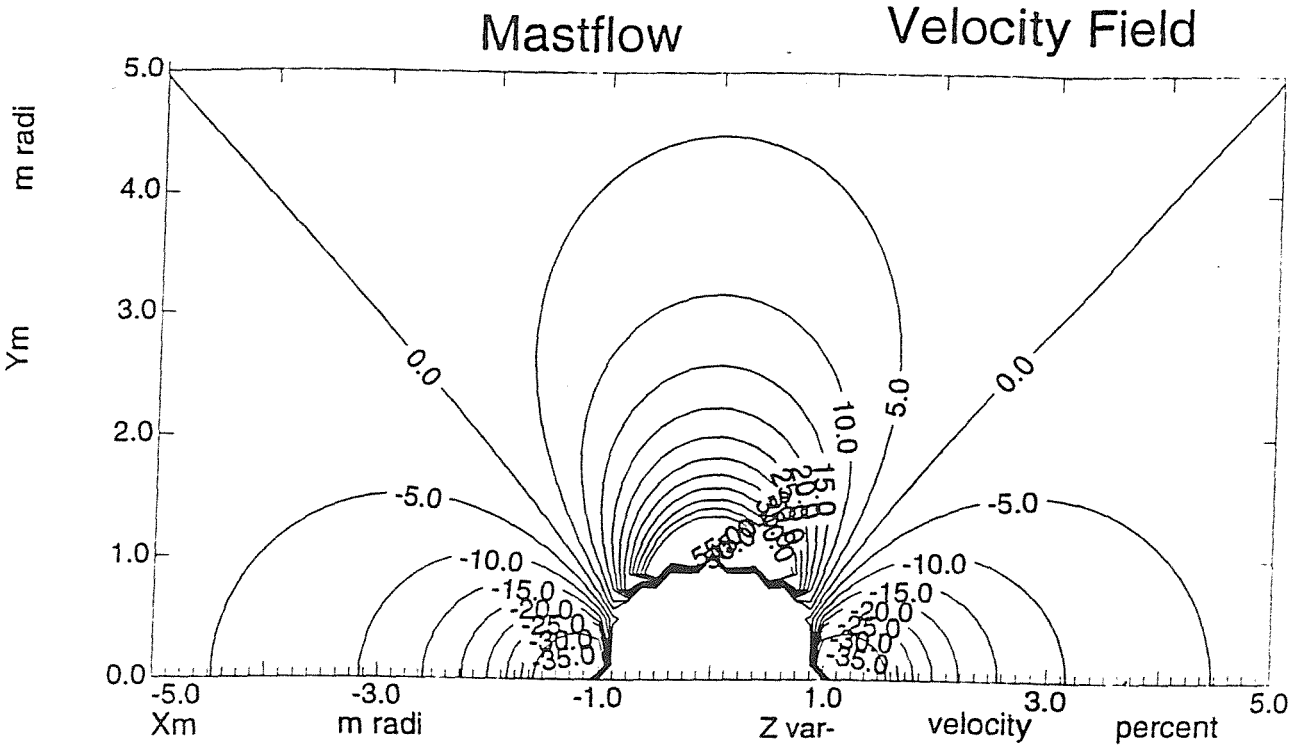

Figure 7 The Percentage change from the free stream velocity for the no wake solution around a cylindrical mast of unit radius. This shows a symmetric profile with error free contours at approx. 45 and 135 degrees, and maximum velocity region at 90 degrees to the flow

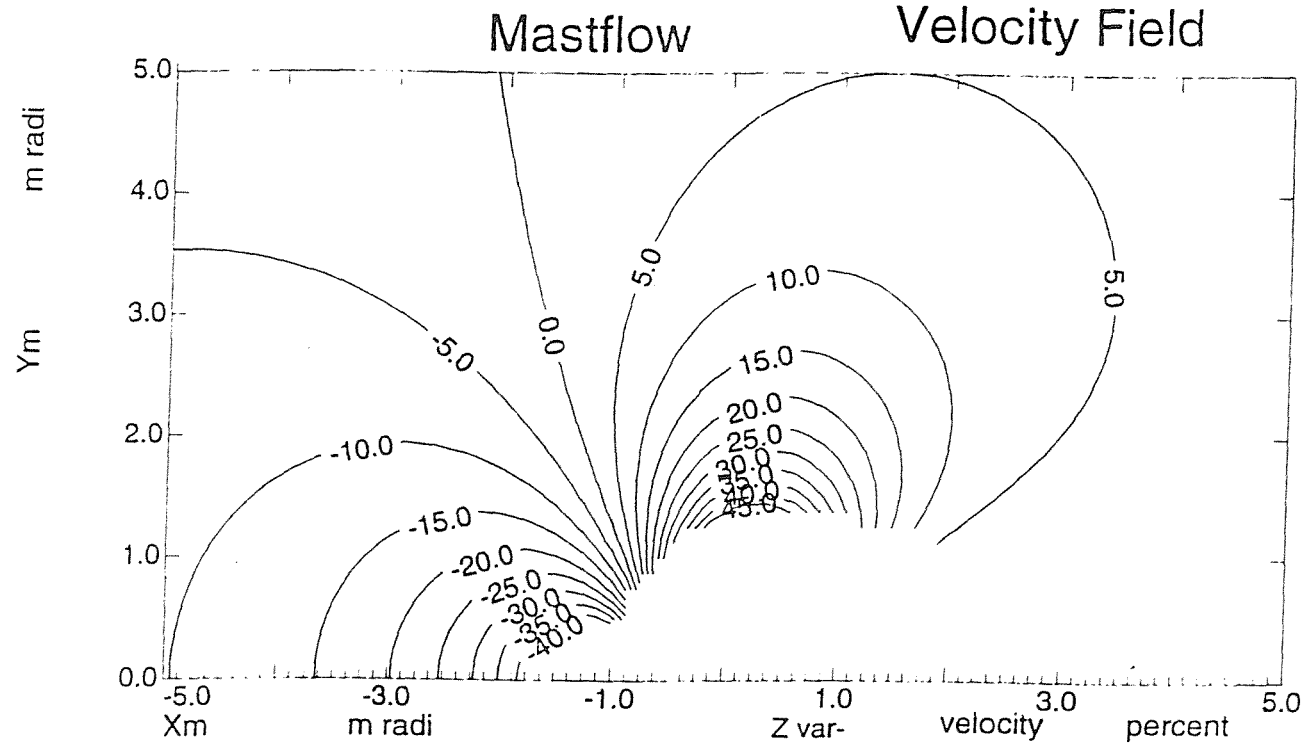

Figure 8 The Percentage change from the free stream velocity for wake potential solution around a cylindrical mast of unit radius. This shows a non-symmetric profile with an error free contour approaching 90 degrees, and maximum velocity region downstream of the flow.

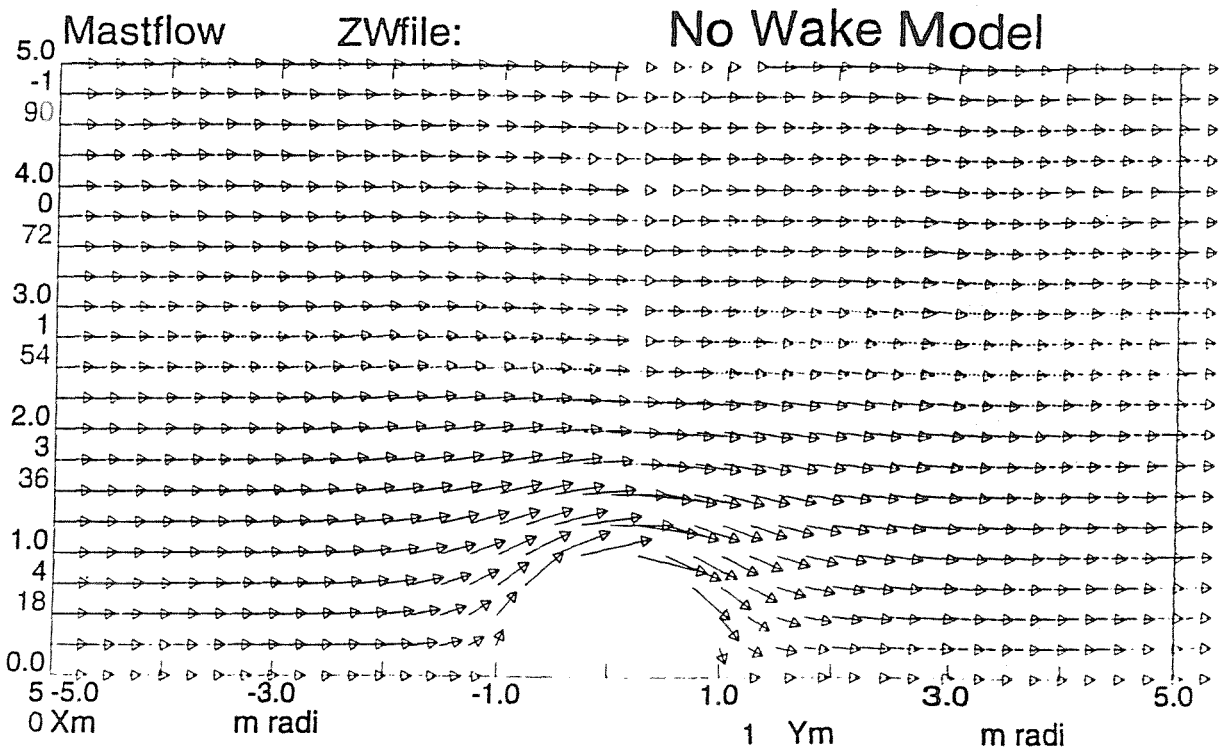

Figure 9 Flow distortion around a cylindrical mast of unit radius for the simple potential solution where the cylindrical drag coefficient = 1.0.

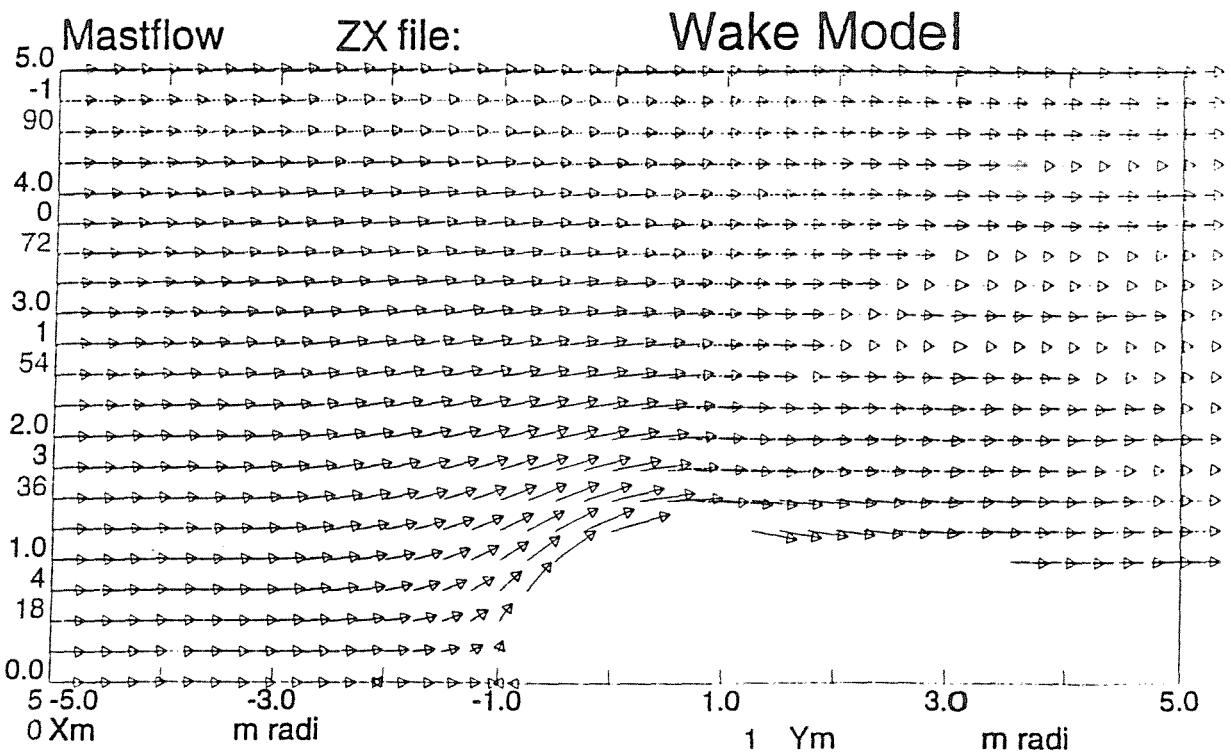

Figure 10 The flow distortion around a cylindrical mast of unit radius for the wake potential solution where C_D=1.0.

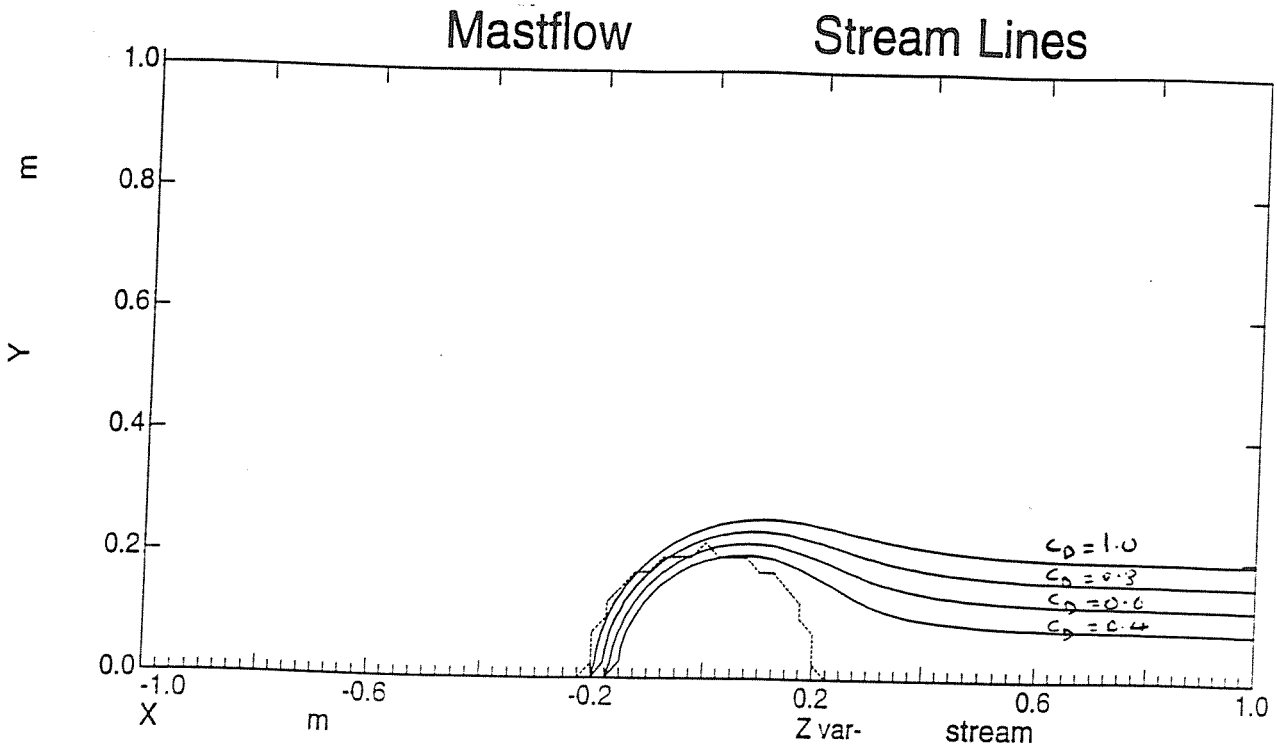

Figure 11 The wake region contours and offsets calculated by the wake potential model for a varying cylindrical drag coefficient.

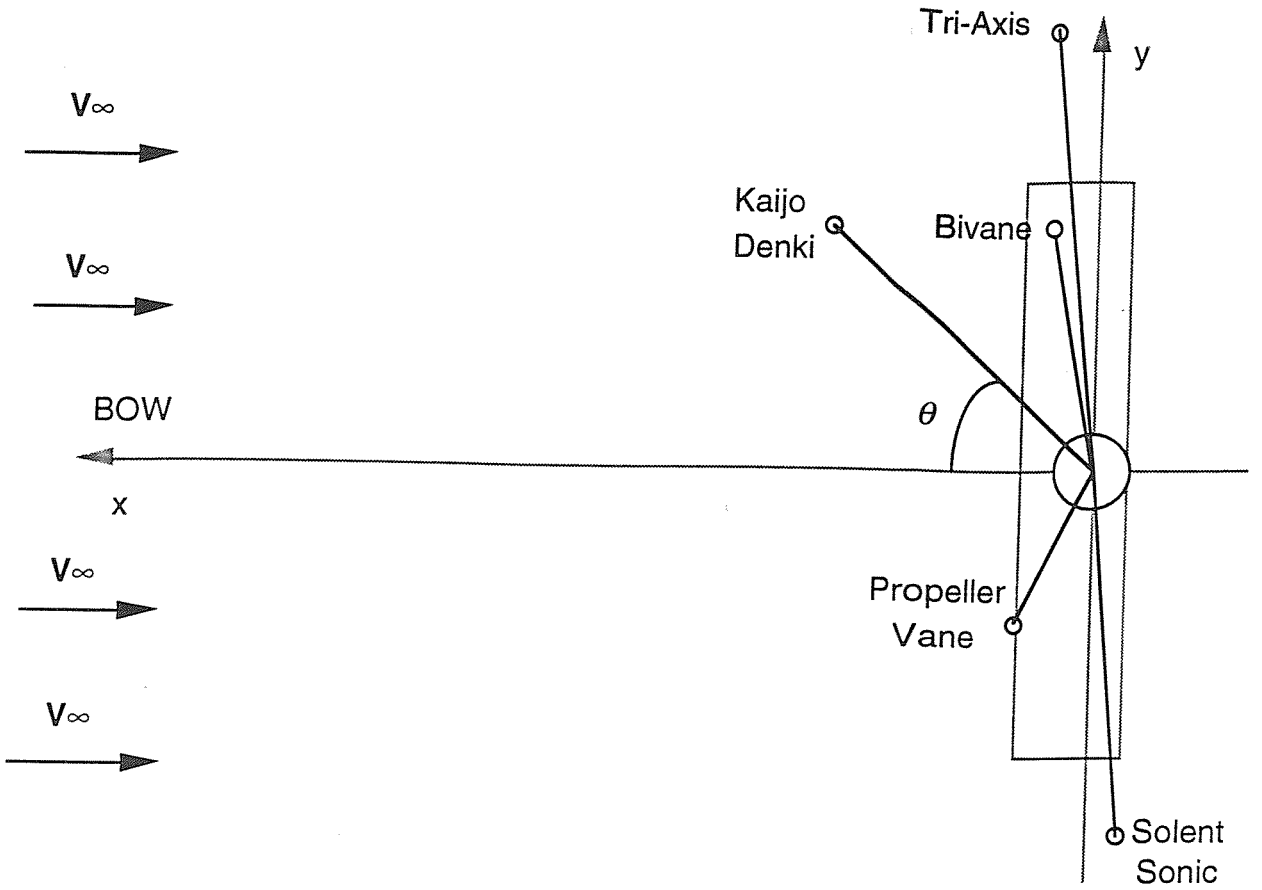

Figure 12 Anemometer positions on R.S.S. Charles Darwin Cruise 43.

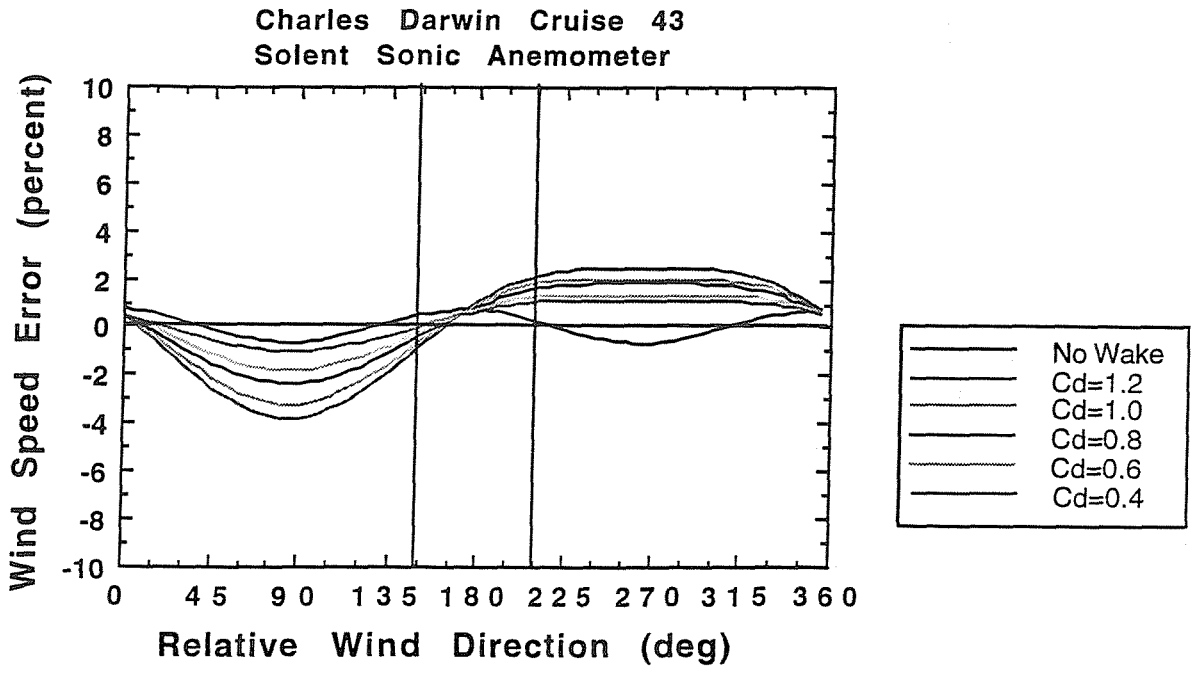

Figure 13 Wind speed errors for the Solent Sonic Anemometer.

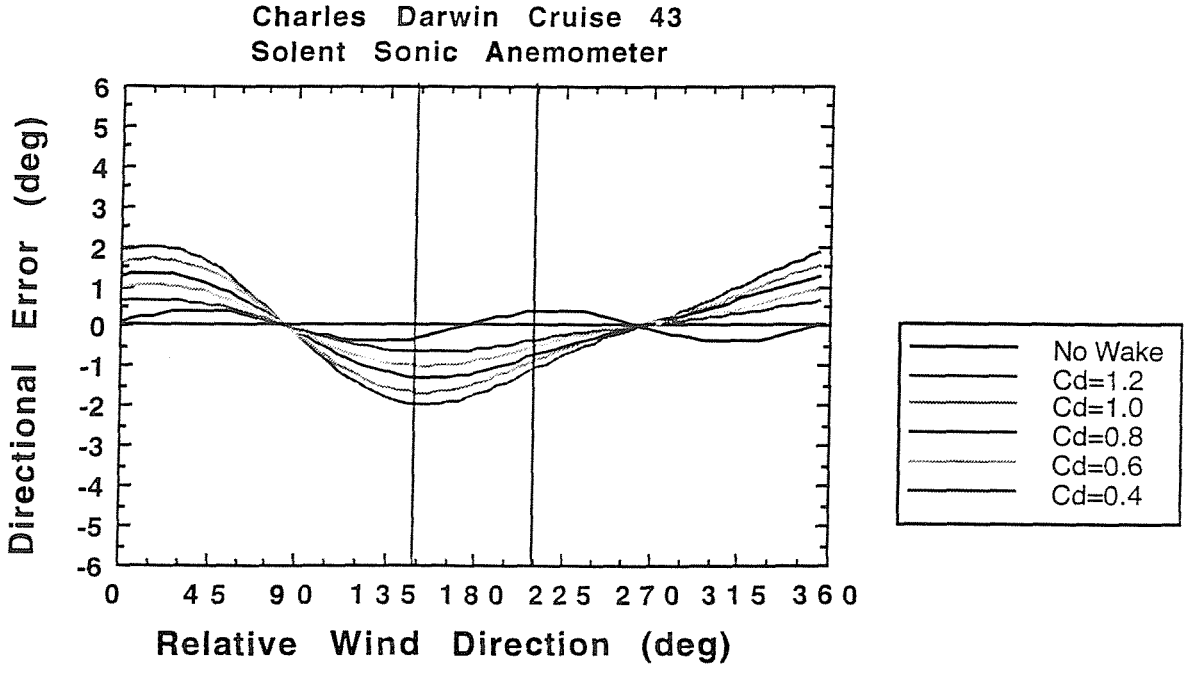

Figure 14 Directional errors for the Solent Sonic Anemometer.

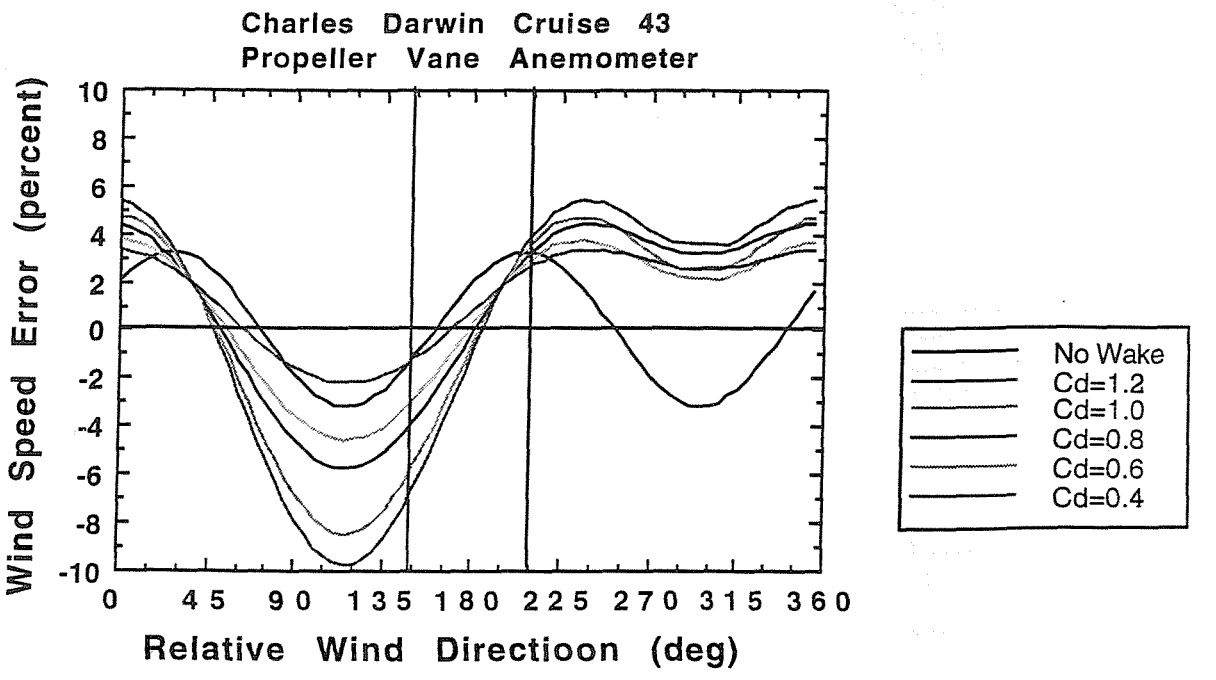

Figure 15 Wind speed errors for the Young Propeller Vane Anemometer.

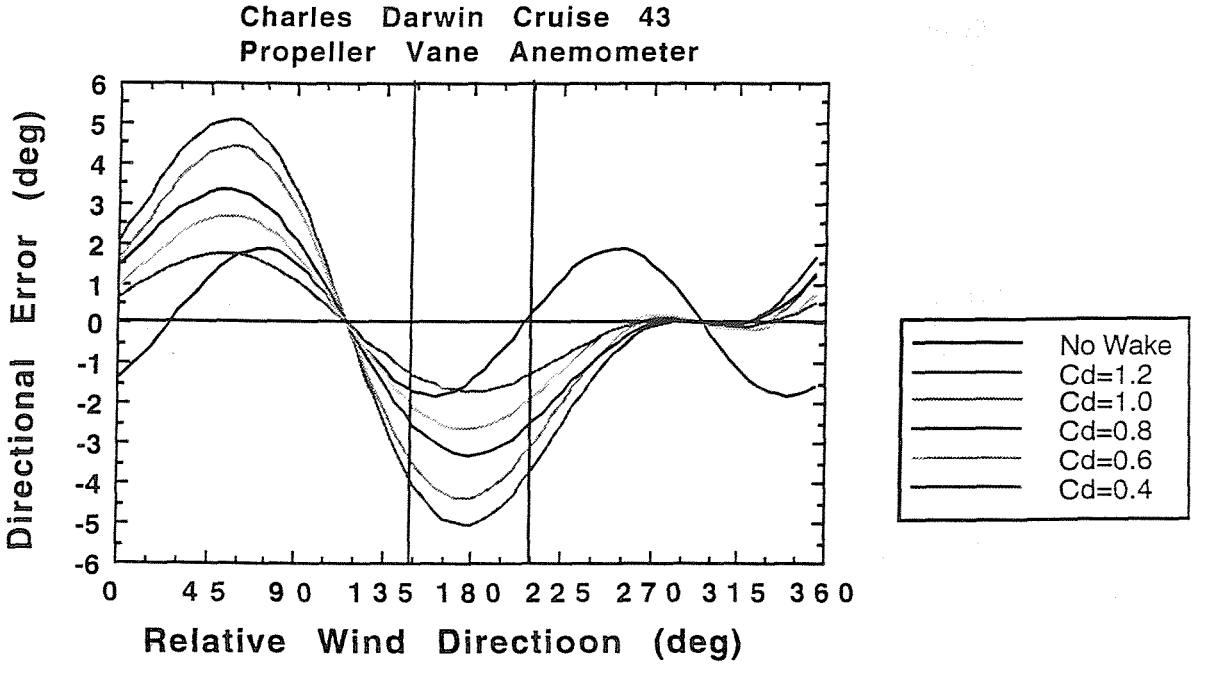

Figure 16 Directional errors for the Young Propeller Vane Anemometer.

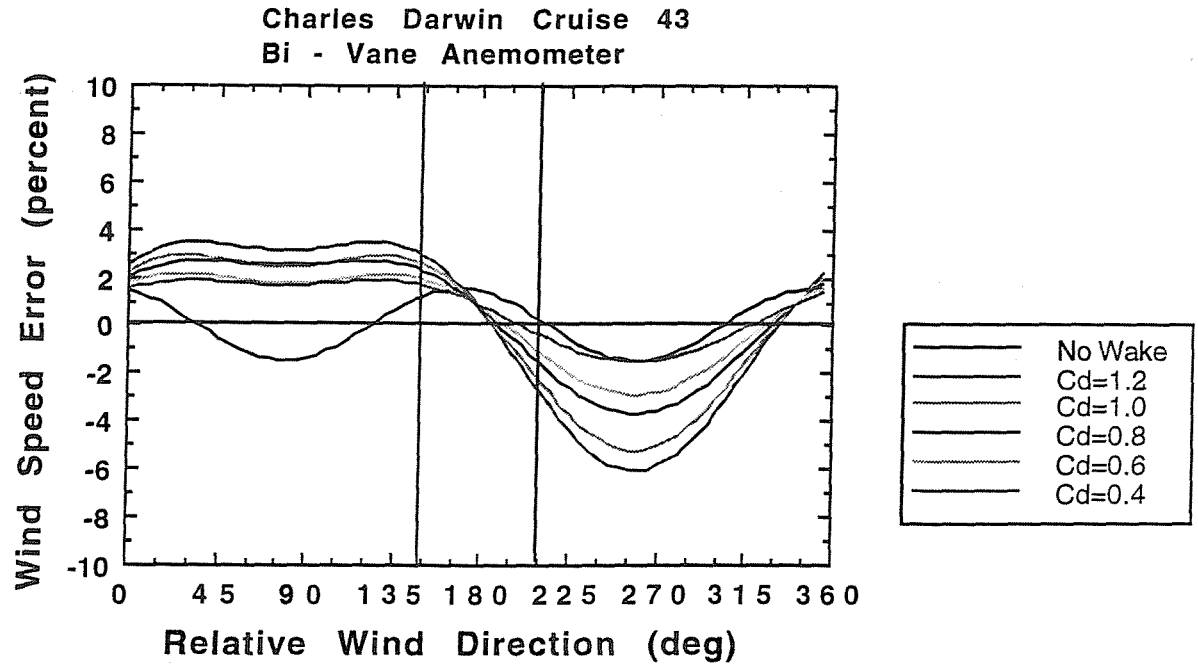

Figure 17 Wind speed errors for the Young Bi - Vane Anemometer.

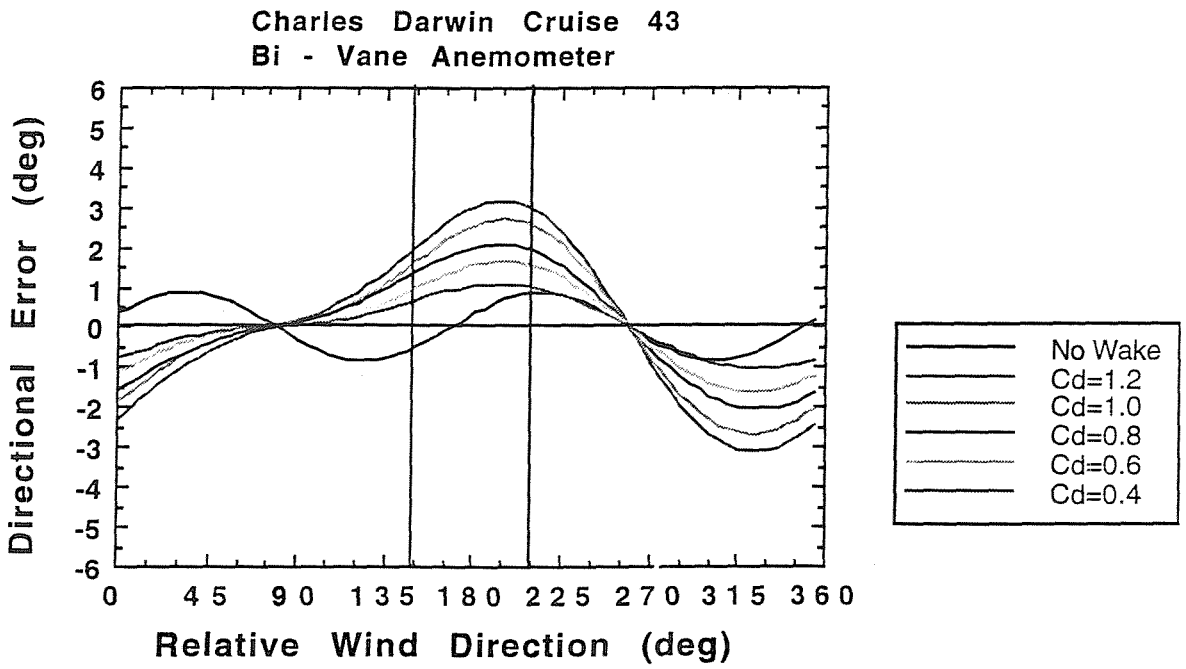

Figure 18 Directional errors for the Young Bi - Vane Anemometer.

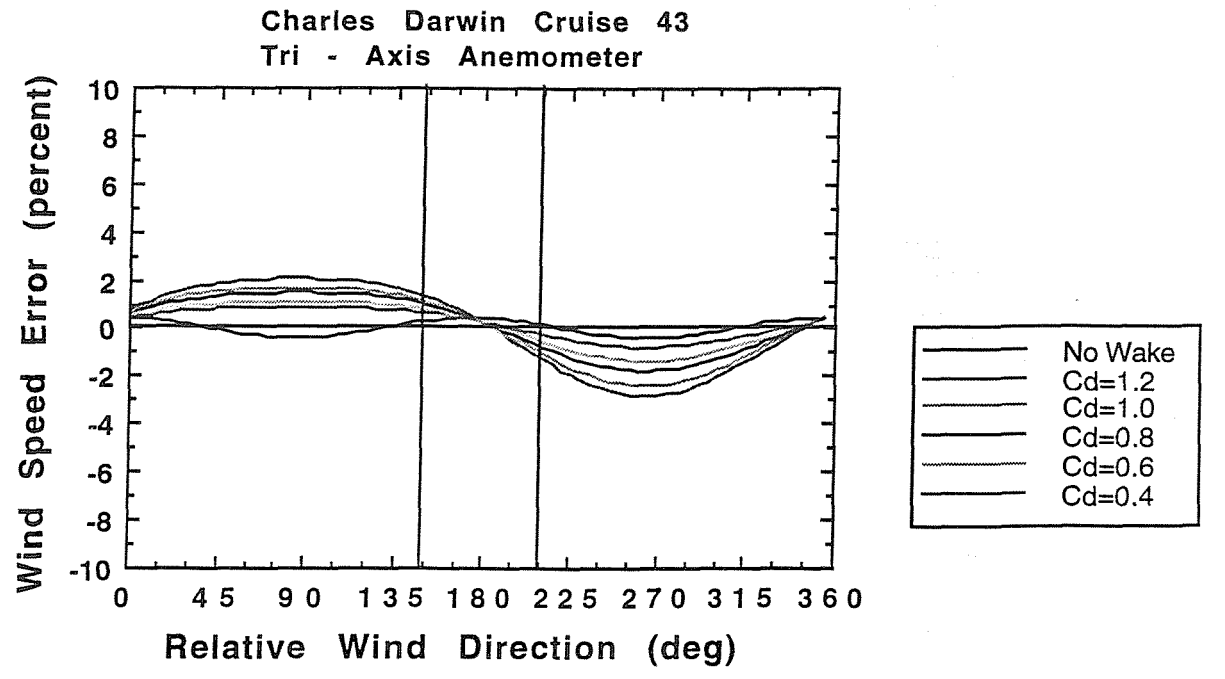

Figure 19 Wind speed errors for the Young Tri - Axis Anemometer.

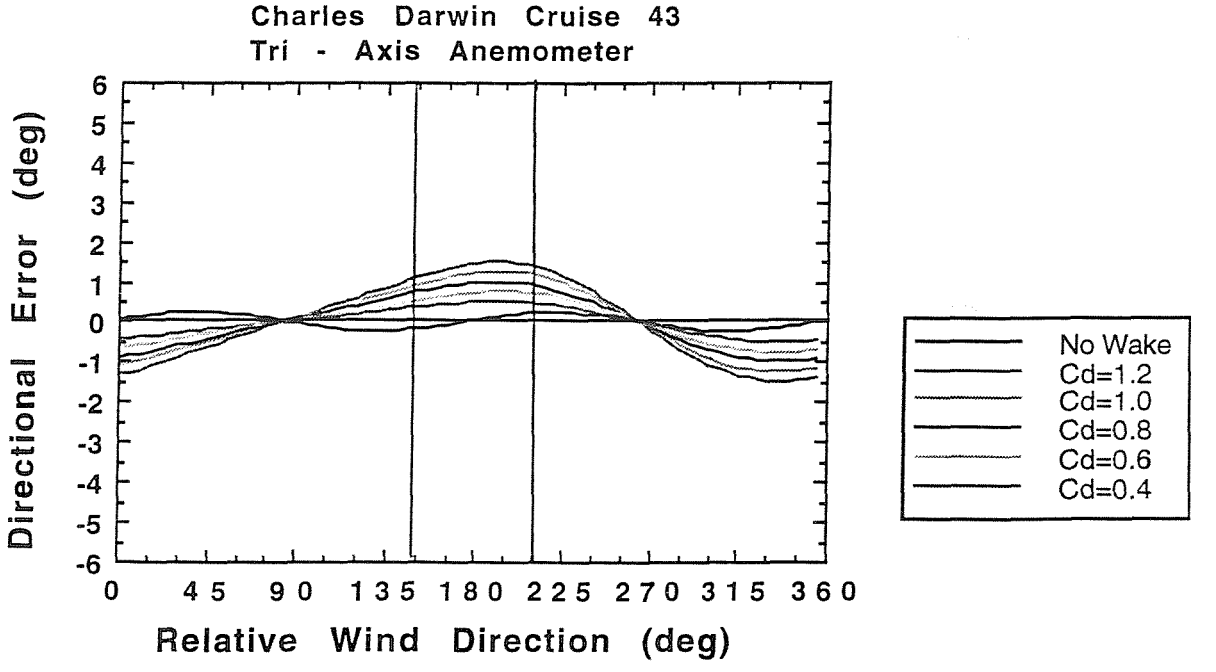

Figure 20 Directional errors for the Young Tri - Axis Anemometer.

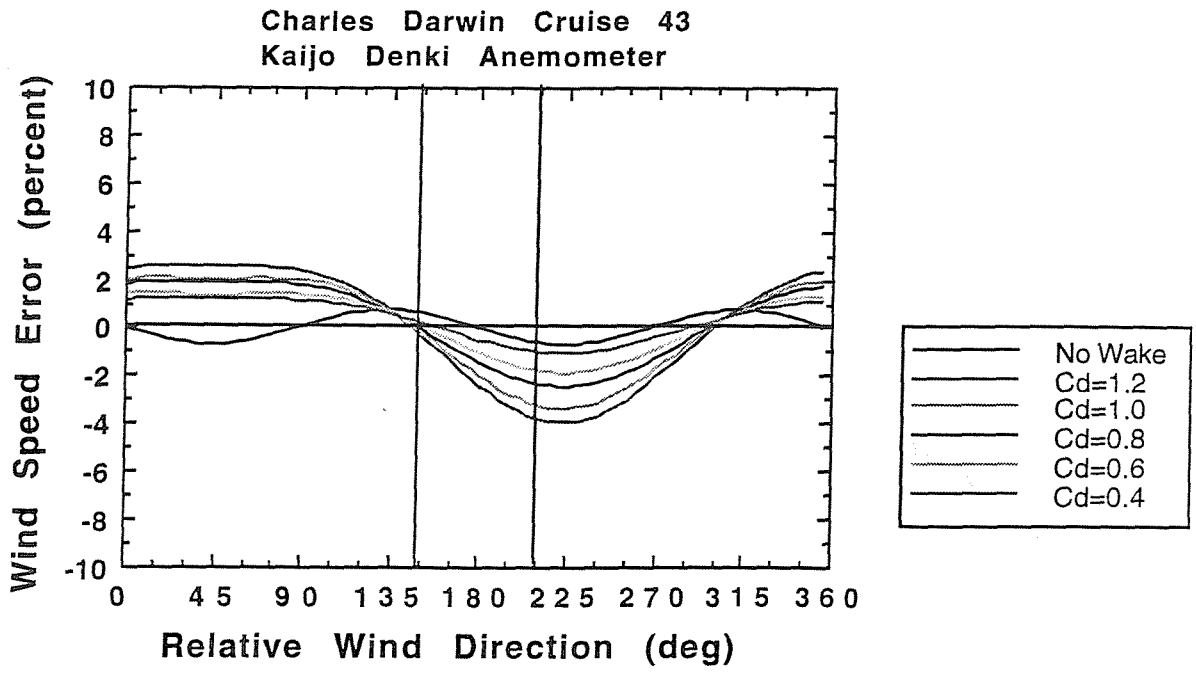

Figure 21 Wind speed errors for the Kaijo Denki Anemometer.

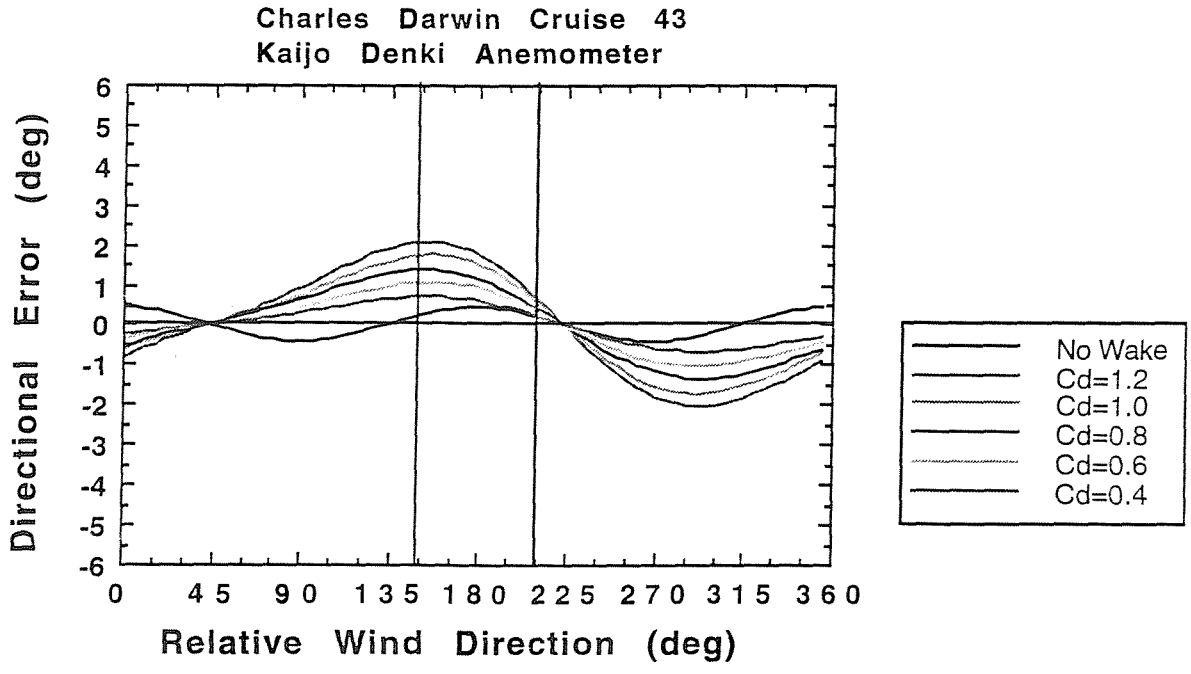

Figure 22 Directional errors for the Kaijo Denki Anemometer.

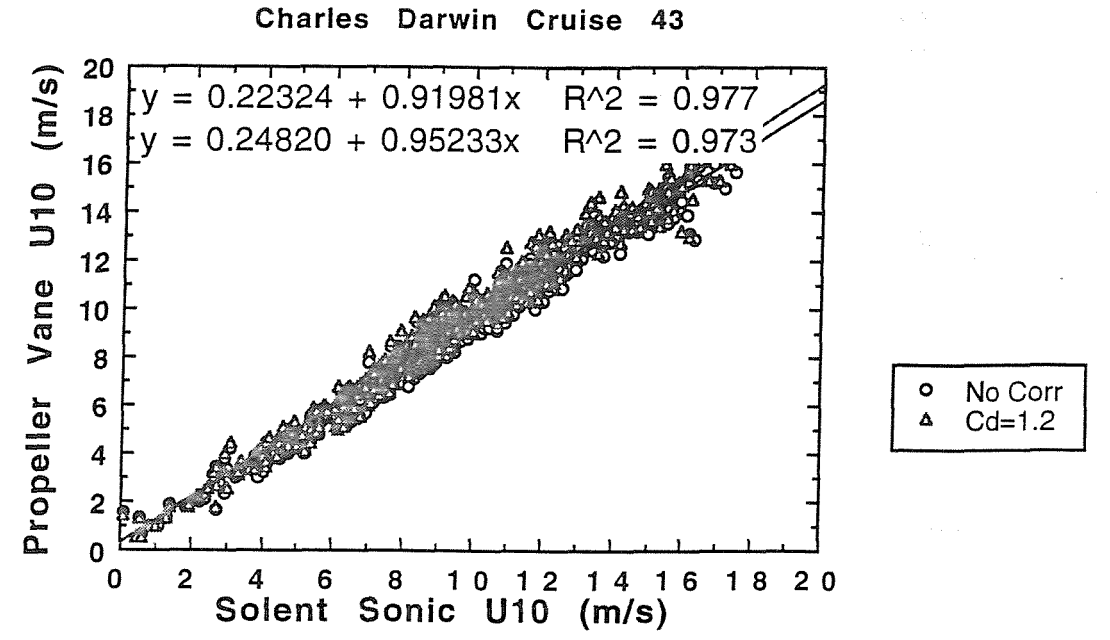

Figure 23 The Solent Sonic vs the Young Propeller for none corrected and model corrected normalised wind speed showing a drop in correlation for the corrected data.

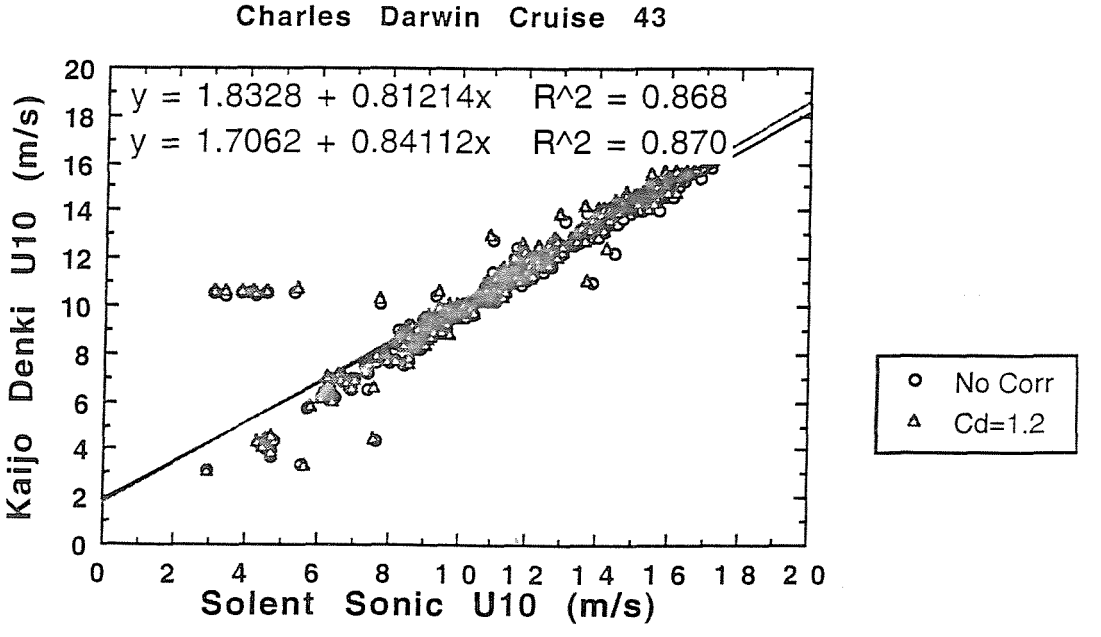

Figure 24 The Solent Sonic vs Kaijo Denki Sonic for none corrected and model corrected normalised wind speed showing an increase in correlation for the corrected data.

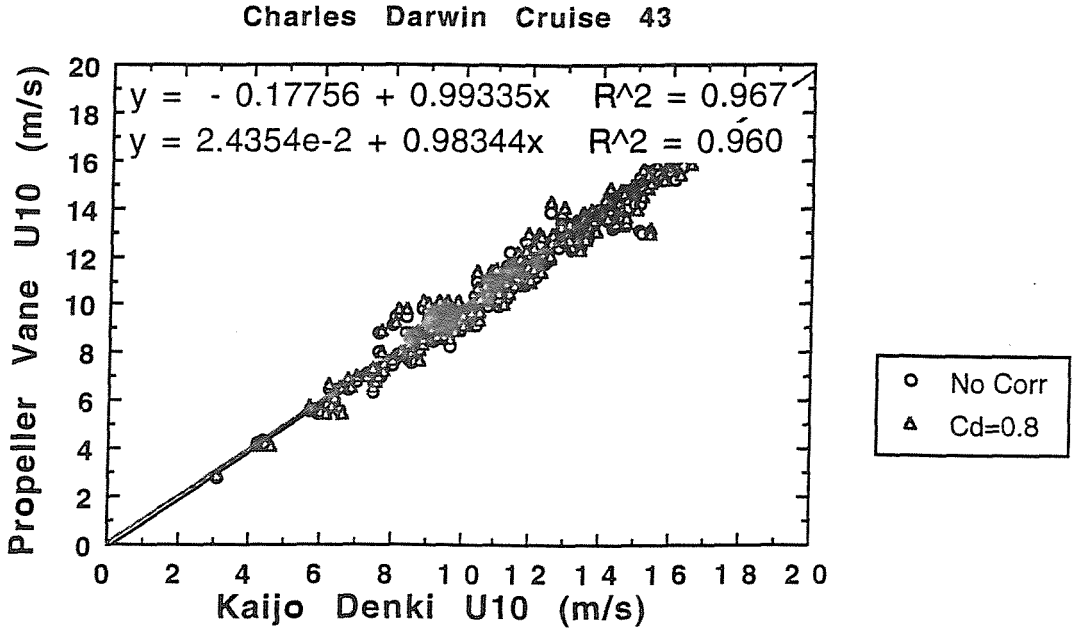

Figure 25 The Kaijo Denki Sonic vs The Young Propeller Vane for none corrected and model corrected normalised wind speed showing a drop in correlation for the corrected data.

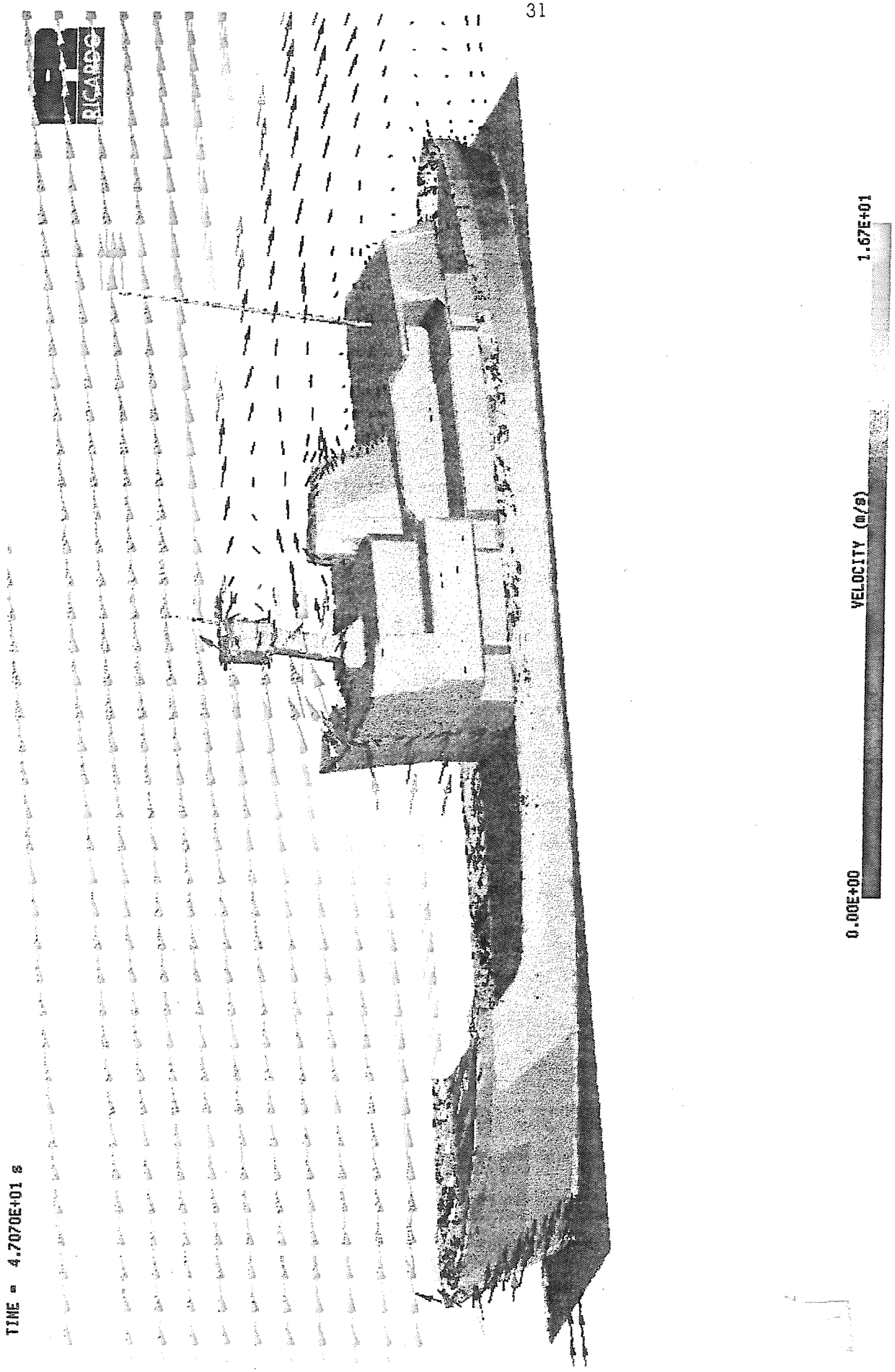

Figure 27 Air flow over the C.S.S. Dawson determined by C.F.D. modelling.

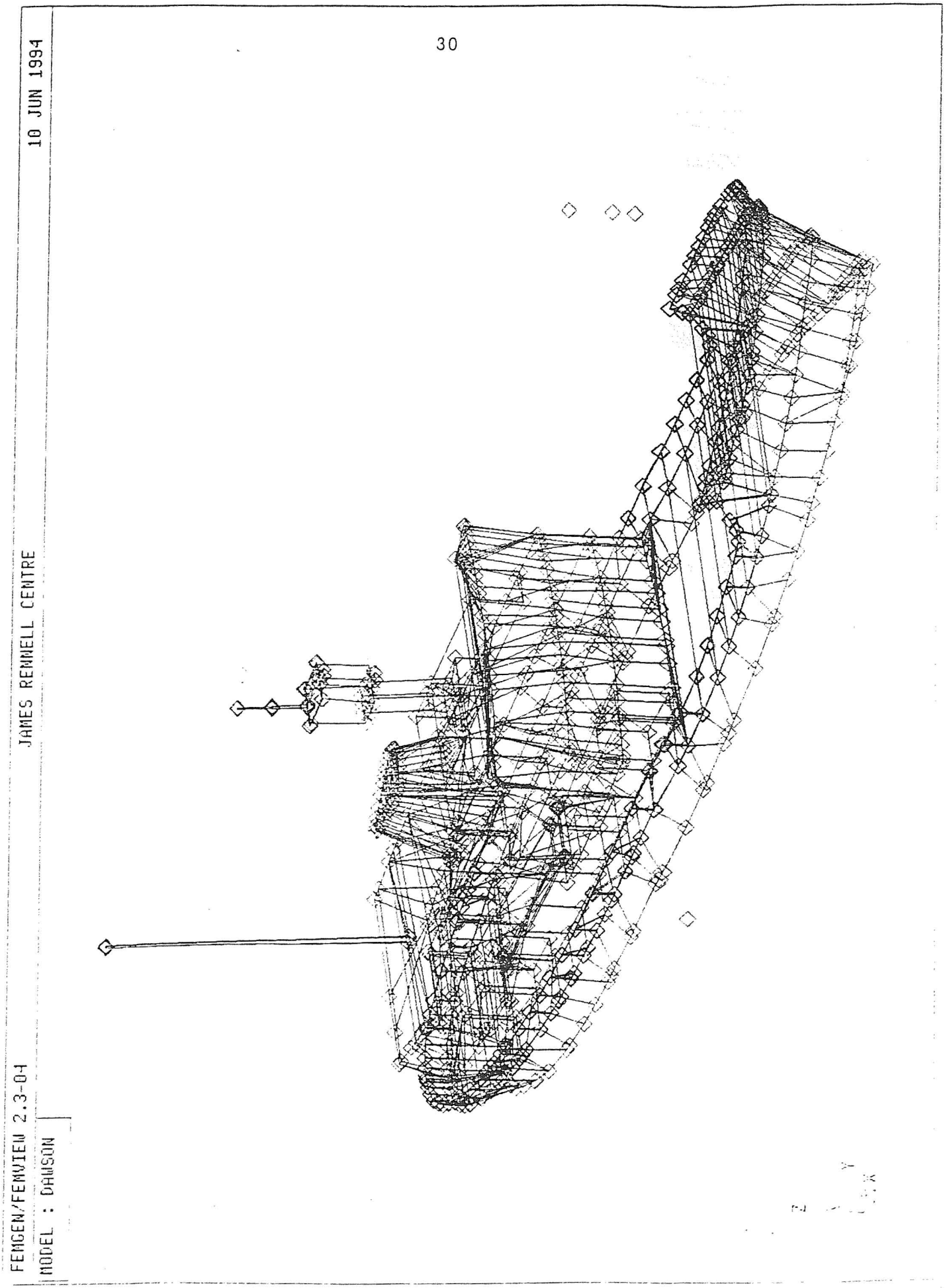

Figure 26 Surface Geometry and Anemometer sites of C.S.S. Dawson produced by the Finite element pre-processor Femgen.

10. TABLES

Charles Darwin Cruise 43				
Drag Coefficient C_D	Mast radius r_o (m)	Source Y_1	Sink Y_2	Offset a_0 (m)
1.0	0.2	1.4012265	1.2012265	0.0
0.8	0.2	1.2984665	1.1384665	0.025
0.6	0.2	1.1957064	1.0757064	0.025
0.4	0.2	1.0929464	1.0129464	0.05

Table 1 The estimated offset, Y_1 and Y_2 for varying cylindrical drag coefficients.

Anemometer	X (m)	Y (m)	Distance (m)	Distance (mast diam)	Theta (deg)
Solent Sonic	-0.2	2.4	2.4083	6.0208	94.7636
Propeller Vane	0.5	1.0	1.1180	2.7950	63.4349
Bi - Vane	0.3	-1.6	1.6279	4.0698	79.3803
Tri - Axis	0.3	-3.1	3.1145	7.7863	84.4725
Kaijo Denki	1.7	-1.6	2.3345	5.8363	43.2643

Table 2 Anemometer positions in relation to mast centre.

Drag Coefficient	Solent Sonic vs Young Propeller Vane		
	m	c	R^2
Raw	0.91981	0.22324	0.977
No Wake	0.91513	0.26551	0.974
1.2	0.95233	0.26551	0.973
1.0	0.94682	0.24820	0.973
0.8	0.93791	0.23772	0.975
0.6	0.93235	0.23840	0.975
0.4	0.92337	0.23013	0.976

Table 3 Regression lines for Solent Sonic Anemometer vs the Young Propeller Vane Anemometer

Drag Coefficient	Solent Sonic vs Kaijo Denki Sonic		
	m	c	R^2
Raw	0.81214	1.8328	0.868
No Wake	0.81857	1.7916	0.869
1.2	0.84112	1.7062	0.870
1.0	0.83715	1.7217	0.870
0.8	0.83155	1.7442	0.869
0.6	0.82763	1.7598	0.869
0.4	0.82228	1.7814	0.896

Table 4 Regression lines for Solent Sonic vs Kaijo Denki Sonic.

Drag Coefficient	Kaijo Denki Sonic vs Young Propeller Vane		
	m	c	R^2
None Corrected	0.99335	-0.17756	0.967
No Wake	0.97541	$-2.6650*10^{-2}$	0.963
1.2	0.98242	0.14377	0.952
1.0	0.98300	0.10316	0.955
0.8	0.98344	$2.4354*10^{-2}$	0.960
0.6	0.98335	$-9.5225*10^{-3}$	0.962
0.4	0.98225	$-7.2240*10^{-2}$	0.964

Table 5 Regression lines of wind speed for Kaijo Denki Sonic anemometer vs Young Propeller Vane anemometer.

11. APPENDIX A - THE JAMES RENNELL CENTRE

1. THE NEED FOR OCEANOGRAPHIC RESEARCH

Oceanography is influencing our everyday lives; not only is it useful for seamen to possess detailed knowledge of the oceans, surface currents and winds but it is evident that the oceans are an integral part of the world climate system. The oceans can transport and store vast amounts of energy and can therefore determine the time scale and regional patterns of climate change. Solar energy is absorbed at the equator and warms the water which is transported towards the poles, were it cools and sinks, and flows back towards the equator. The heat from this process is distributed into the atmosphere, which influences the winds, rainfall patterns and regional temperatures.

1.1 THE JAMES RENNELL CENTRE FOR OCEAN CIRCULATION

The Natural Environment Research Council (N.E.R.C.) was formed in 1965. Its purpose was to combine all the different environment agencies under the management and funding of one central body. The National Institute of Oceanography combined with the Institute of Coastal Oceanography and Tides and the Unit of Coastal Sedimentation in 1973, to become the Institute of Oceanographic Sciences Deacon Laboratory (I.O.S.D.L.), which remains in Surrey to this day. In the spring of 1990 it was announced that the James Rennell Centre for Ocean Circulation (J.R.C.) was to be established at Southampton as a component of the I.O.S.D.L. It opened in December 1990, and is now being managed independently to I.O.S.D.L. Its purpose is to manage and support the U.K. contribution to the World Ocean Circulation Experiment (W.O.C.E.). The W.O.C.E. is part of the World Climate Research Programme. It is the largest ever international study of the physics of the ocean and its role in the climate of our planet. It involves scientists from over forty nations using satellites, ships, buoys and floats.

The J.R.C. has a staff of about fifty, some of whom are based at the I.O.S.D.L., who are split up into six scientific teams with support from an administrative team. The Survey team enables frequent cruises to be supported and undertakes acquisition and processing of data to high standards both at sea and at the J.R.C. The Tracer Chemistry team concentrates on the measurement and distribution of oxygen, silicate, phosphate, nitrate; the chlorofluorocarbons CFC-10, CFC-11, CFC-12 and CFC-13, and plant pigments within the oceans. The Biological team is producing models with the aim of predicting nitrogen and carbon cycles from plankton and zooplankton activity in the upper ocean. The Satellite team is developing techniques for processing images of the oceans taken from satellites such as ERS - 1 and TOPEX/POSIDEN. The satellites can measure sea surface temperature, wind velocity, wave height and slopes in sea level, which relate to ocean currents. The Physical Modelling team is developing the Atlantic Isopycnic Model (A.I.M.), which is being used to examine the coupling between the upper ocean and the ocean interior and the role of eddies in ocean circulation.

The James Rennell Centre, I.O.S.D.L., Southampton University Department of Oceanography and Research Vessel Services are going to be combined into one new dockside centre, in Southampton in 1995, called the Southampton Oceanography Centre.

1.2 THE SURFACE METEOROLOGY TEAM

Until April 1994 the Surface Meteorology team was split into the Ocean Instrumentation Group, based at the I.O.S.D.L., whilst the data analysis group is situated at the J.R.C. The Ocean Instrumentation group is now known as the Centre for Ocean Technology Development (C.O.T.D.), leaving five members in the Meteorological team at the J.R.C.

The Surface Meteorology teams primary role is to understand how the ocean controls and responds to the weather in the atmosphere. Values for the transfers (or fluxes) of heat, water, and momentum between the ocean and the atmosphere are calculated and used to verify climate models of the coupled ocean atmosphere system.

12. APPENDIX B - SHIP MODELS

The following Appendix contains the ship models created using the Finite Element pre-processor Femgen. The models included are the R.R.S. Challenger, O.W.S. Cumulus, R.R.S. Charles Darwin, C.S.S. Dawson, R.R.S. Discovery, C.S.S. Hudson, Le Suroit and The Warden.

DEL: CHALAL

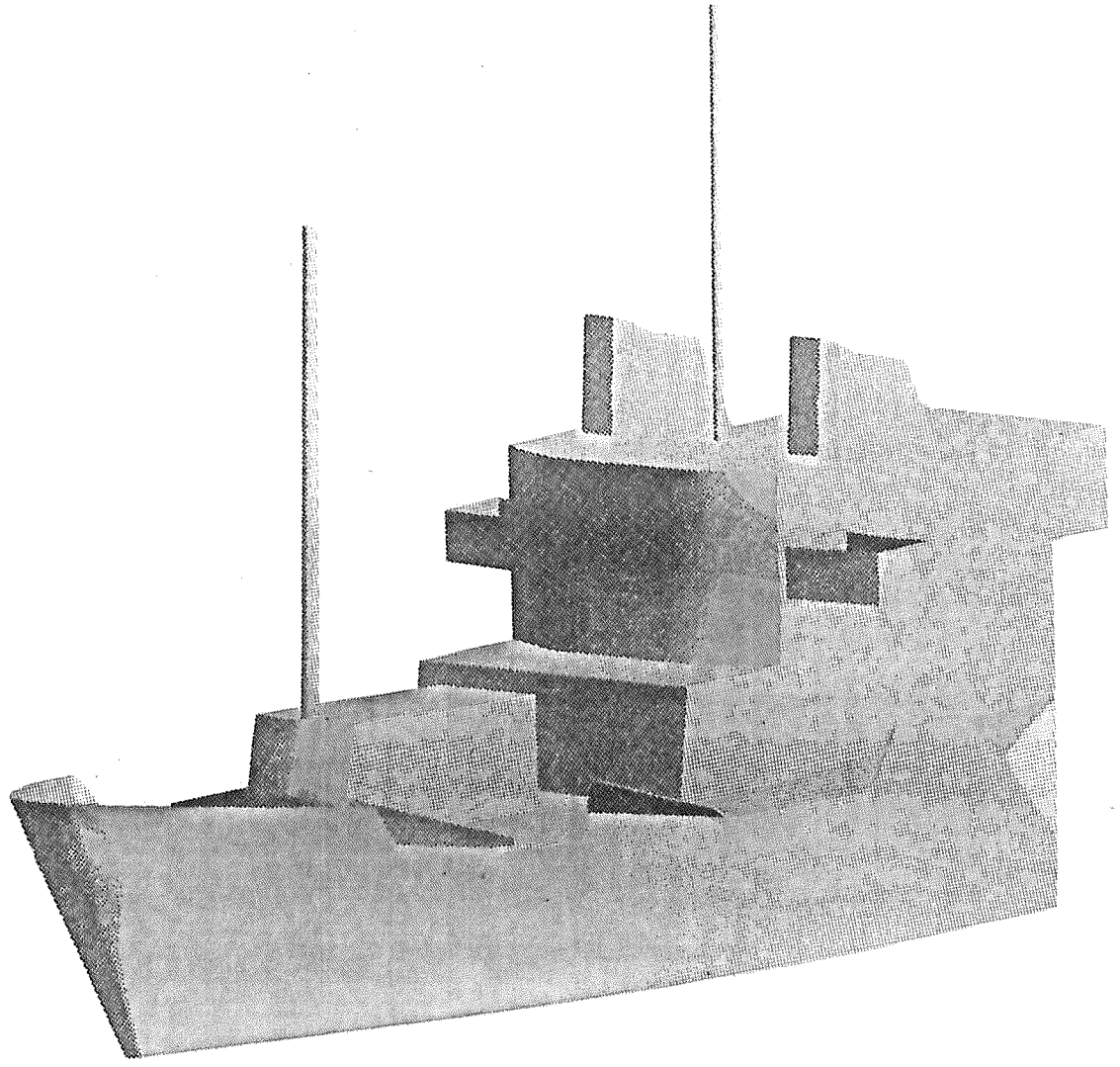

R.R.S. Challenger

DEL: CUMULU

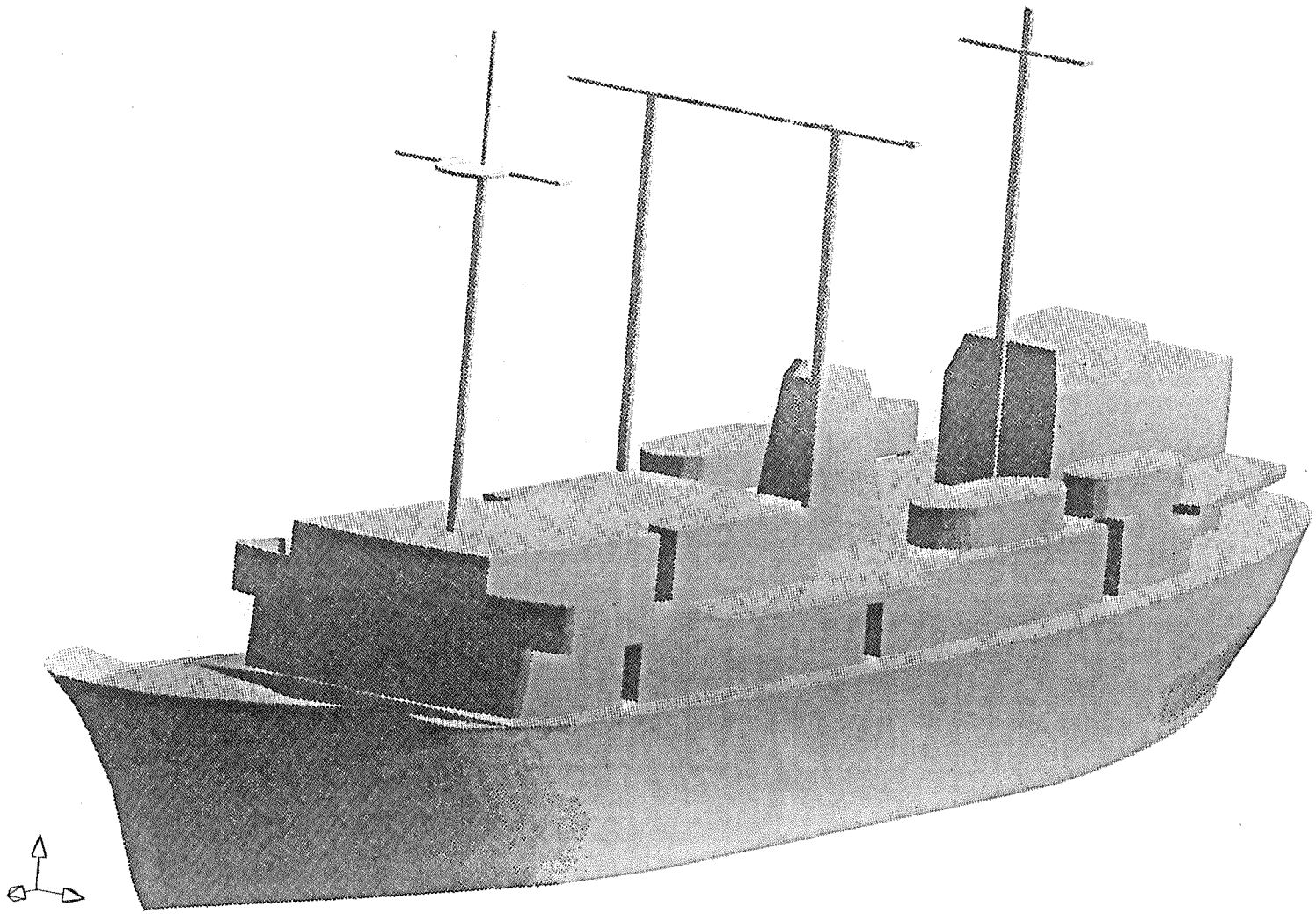

O.W.S. Cumulus

DEL: NEW1

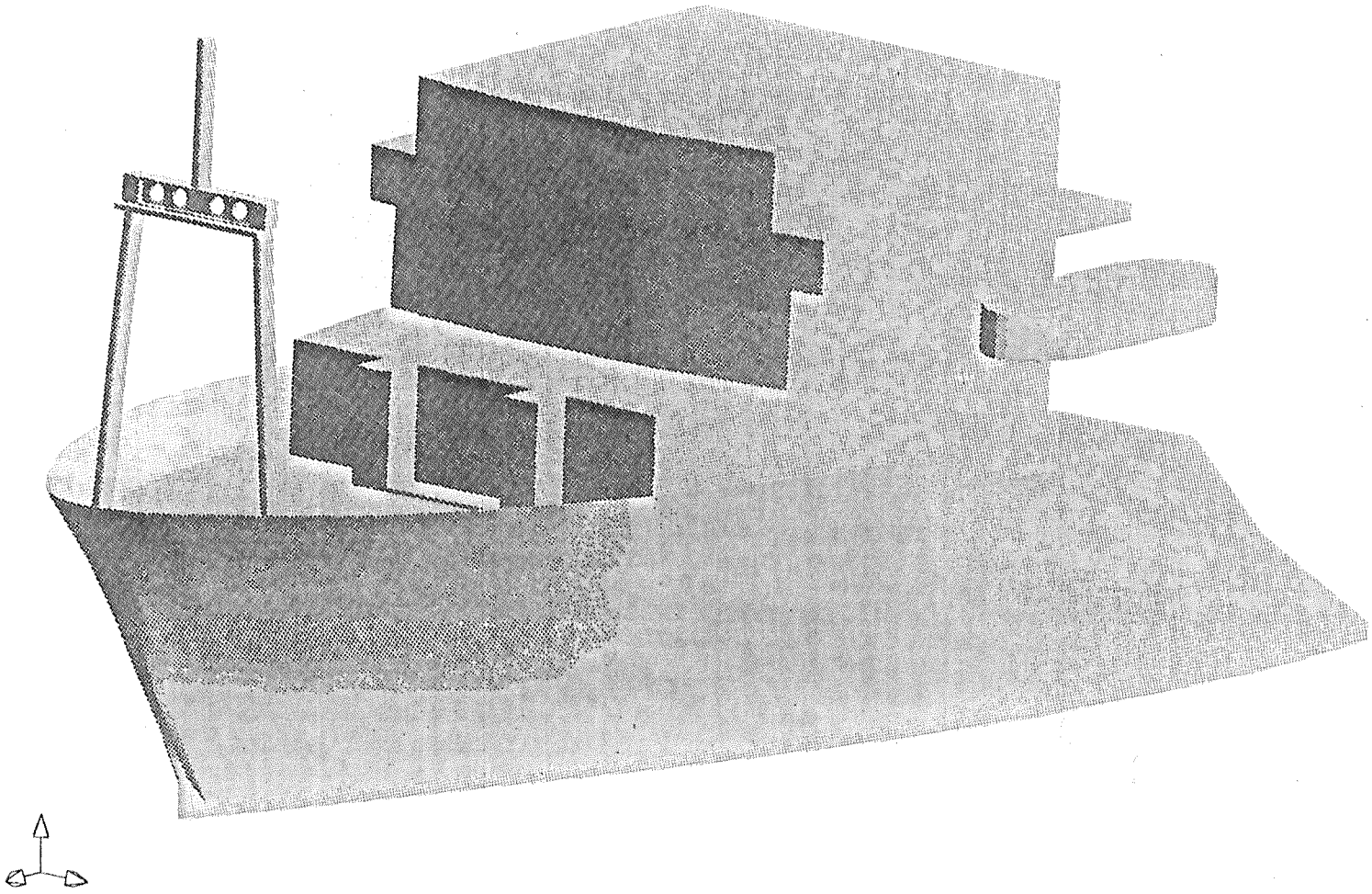

R.R.S. Charles Darwin

DEL: DAWSON

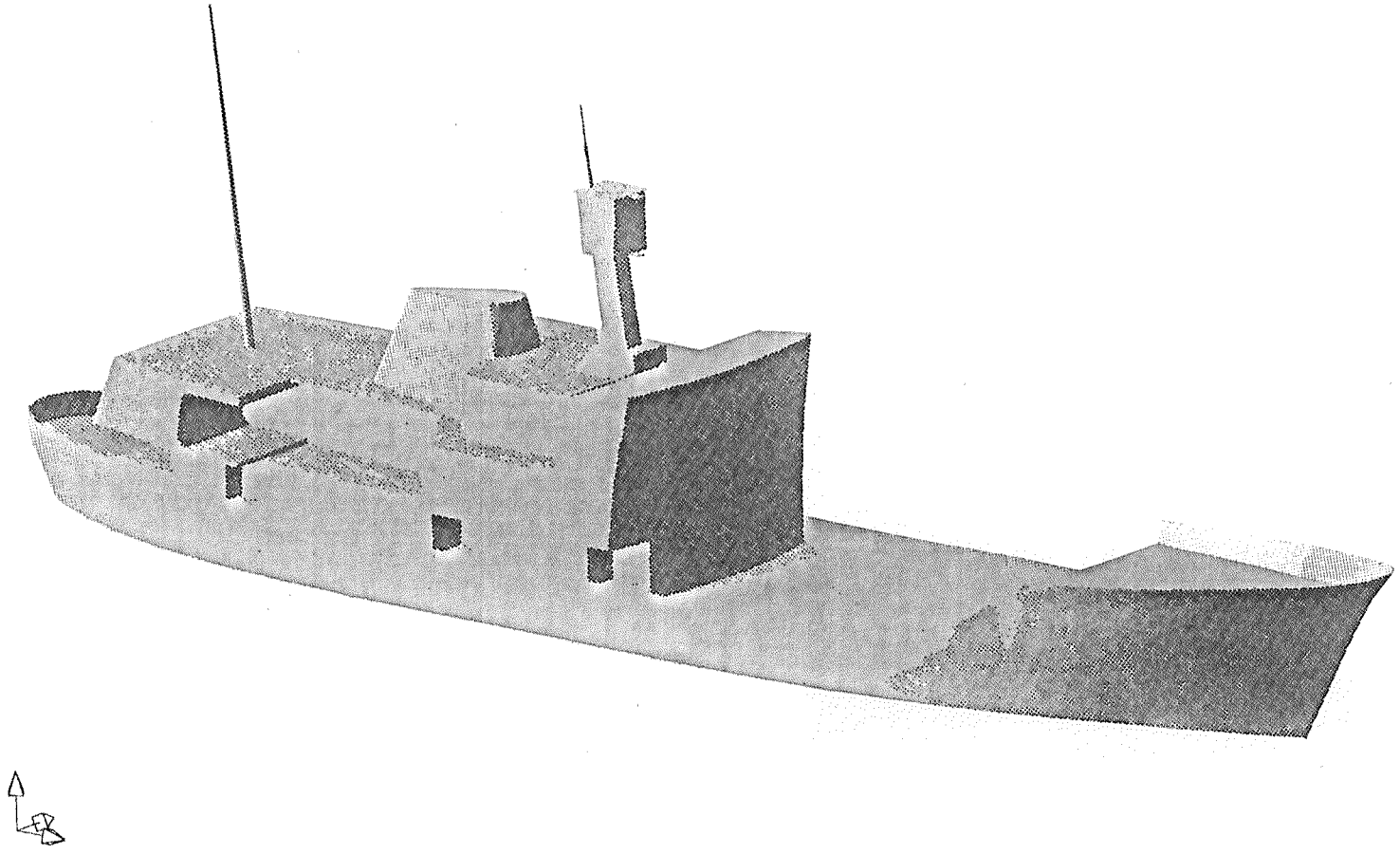

C.S.S. Dawson

DEL: DISCAL

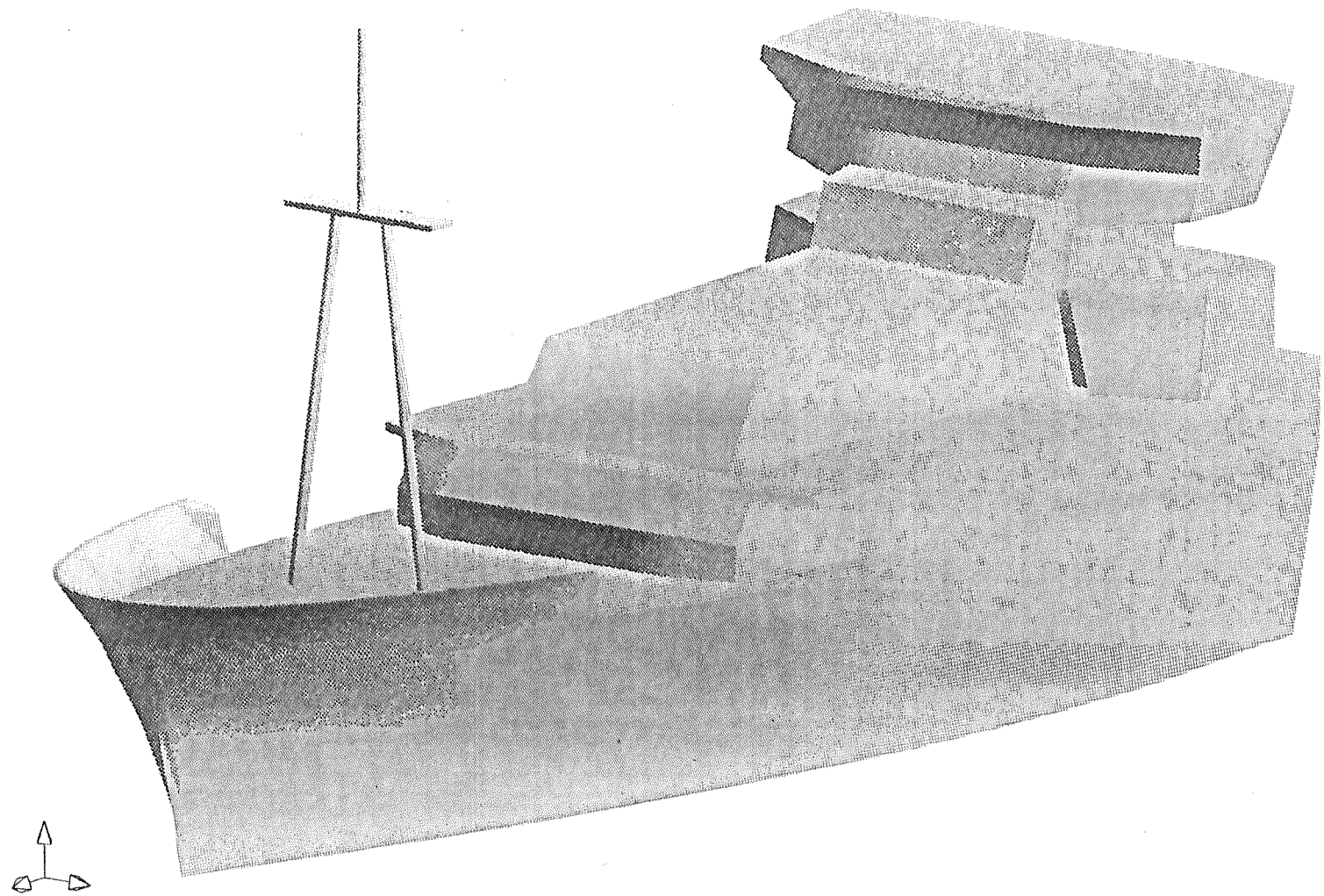

R.R.S. Discovery

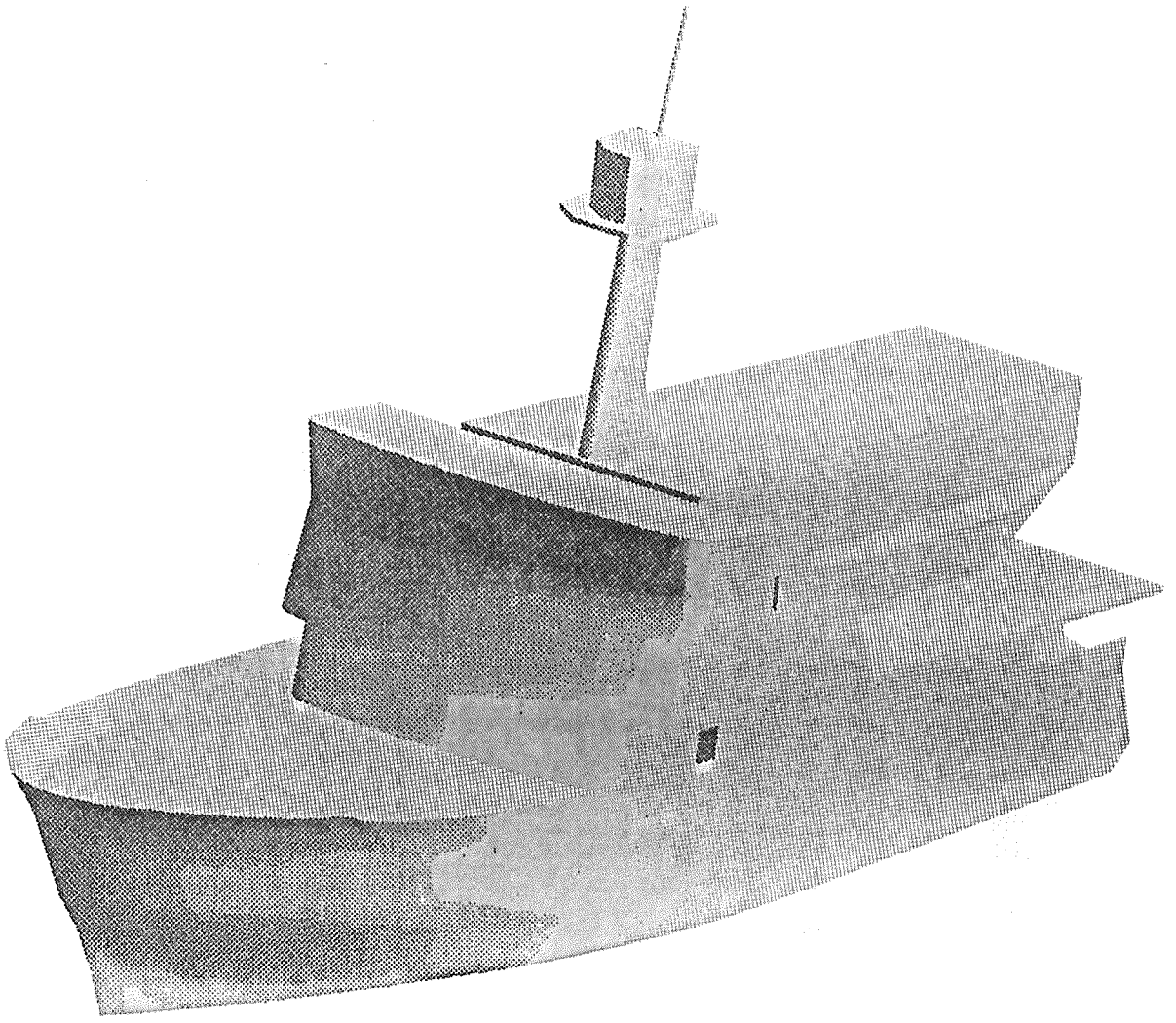

C.S.S. Hudson

DEL: SUROIT

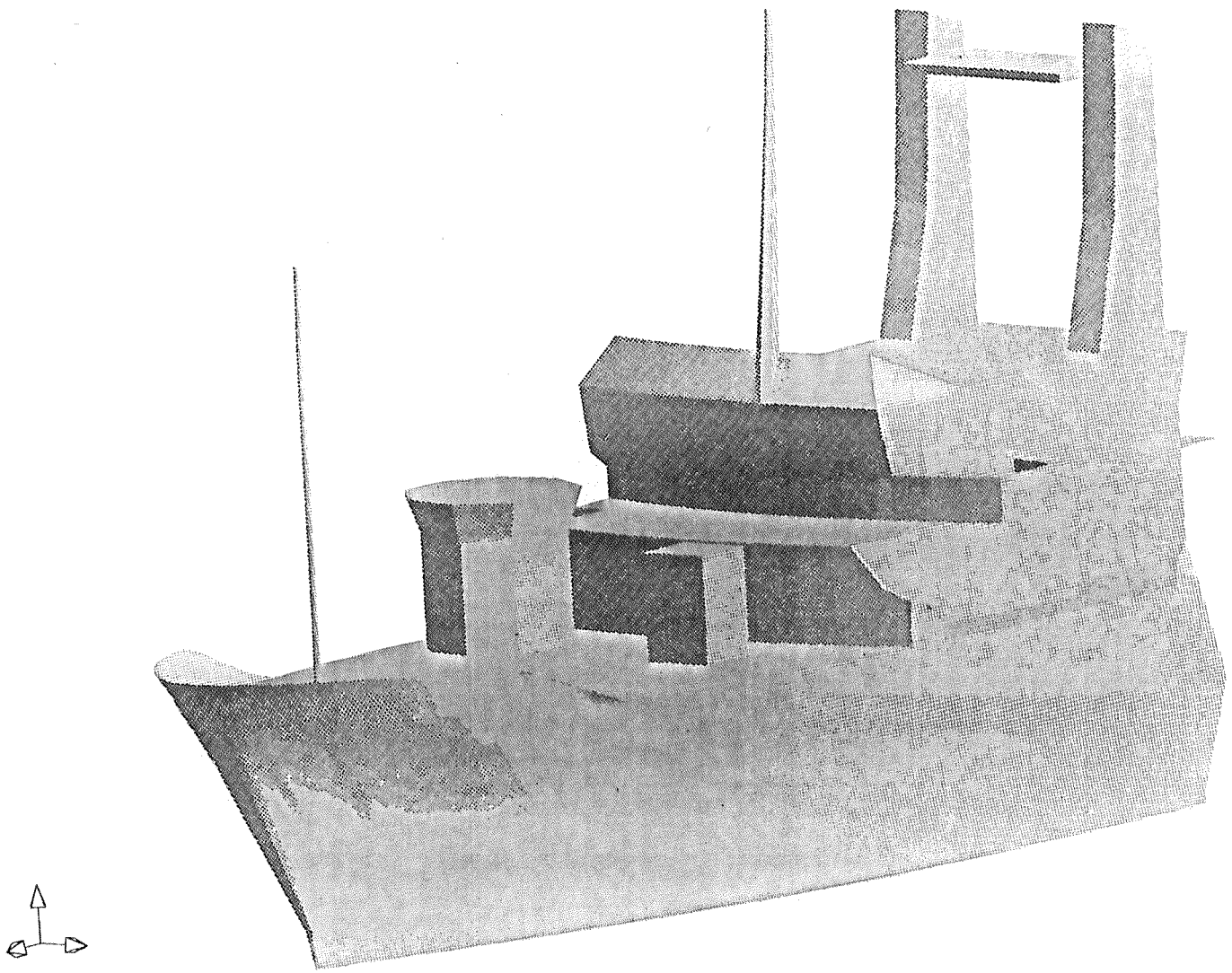

Le Suroit

DEL: WARDSE

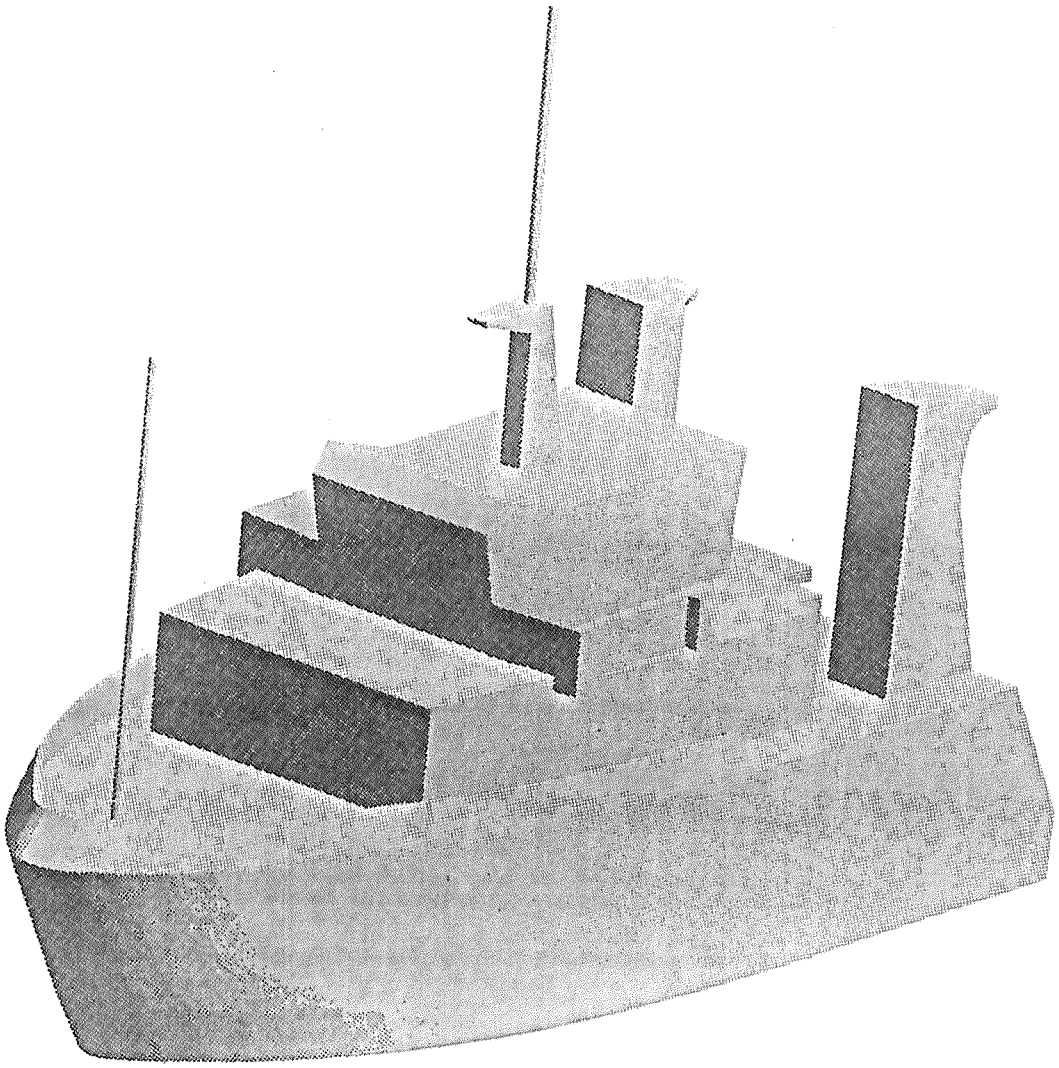

The Warden


Natural
Environment
Research
Council